

# Hybrid STAR-RIS Enabled Integrated Sensing and Communication

Zehra Yigit, *Member, IEEE*, Ertugrul Basar, *Fellow, IEEE*

**Abstract**—Integrated sensing and communication (ISAC) is recognized as one of the key enabling technologies for sixth-generation (6G) wireless communication networks, facilitating diverse emerging applications and services in an energy and cost-efficient manner. This paper proposes a multi-user multi-target ISAC system to enable full-space coverage for communication and sensing tasks. The proposed system employs a hybrid simultaneous transmission and reflection reconfigurable intelligent surface (STAR-RIS) comprising active transmissive and passive reflective elements. In the proposed scheme, the passive reflective elements support communication and sensing links for local communication users and sensing targets situated within the same physical region as the base station (BS), while low-power active transmissive elements are deployed to improve sensing performance and overcome high path attenuation due to multi-hop transmission for distant communication users and sensing targets situated far from the coverage area of the BS. Moreover, to optimize the transmissive/reflective coefficients of the hybrid STAR-RIS, a semi-definite relaxation (SDR)-based algorithm is proposed. Furthermore, to evaluate communication and sensing performance, signal-to-interference-noise ratio (SINR) and Cramer-Rao bound (CRB) metrics have been derived and investigated via conducting extensive computer simulations.

**Index Terms**—Integrated sensing and communication (ISAC), simultaneous transmission and reflection reconfigurable intelligent surface (STAR-RIS), multi-user, multi-target, active RIS.

## I. INTRODUCTION

Sixth-generation (6G) networks are envisioned to provide intelligent, secure, and ubiquitous wireless connectivity via new and enhanced usage scenarios with advanced capabilities [1]. In this vision, integrated sensing and communication (ISAC) stands out as a key enabling technology that offers a unified platform for hardware resources, spectrum, and signal processing framework to enable simultaneous communication and sensing functionalities [1, 2]. This integration brings mutual benefits of communication and sensing via enhancing the hardware, spectrum, energy, and cost efficiencies while defining new sensing-related environmental-aware applications and services, including vehicle-to-everything (V2X), remote sensing, smart cities, smart healthcare, and environmental monitoring [3].

Z. Yigit is with Turkcell 6GEN Lab., Istanbul, Turkiye. E-mail: zehra.yigit@turkcell.com.tr.

E. Basar is with the Department of Electrical Engineering, Tampere University, 33720 Tampere, Finland, on leave from the Department of Electrical and Electronics Engineering, Koc University, 34450 Sariyer, Istanbul, Turkiye. E-mail: ertugrul.basar@tuni.fi and ebasar@ku.edu.tr.

This work was supported by The Scientific and Technological Research Council of Turkiye (TUBITAK) through the 1515 Frontier Research and Development Laboratories Support Program under Project 5229901 - 6GEN. Lab: 6G and Artificial Intelligence Laboratory, and also Grant 120E401.

Although ISAC has gained significant attention in the literature over the past few years, it has a longstanding history of research under various names, such as joint radar and communication (JRC) [4], joint communication and radar (JCR) [5] and dual function radar communication (DFRC) [6]. The primary difference between JRC and JCR lies in their respective emphasis: JRC prioritizes radar-centric designs with integrated communication capabilities, while JCR emphasizes communication-centric designs enhanced with radar functionalities. On the other hand, DFRC refers to a unified platform that utilizes shared waveforms for both communication and sensing tasks [5].

Reconfigurable intelligent surface (RIS)-empowered communication is another emerging technology that offers energy and cost-efficient solutions for ubiquitous connectivity in next generation networks [7, 8]. RISs are planar metasurfaces consisting a large number of passive reflective elements to efficiently modify wireless propagation environment, thereby paving the way of achieving the vision for a smart radio environment [9, 10]. By dynamically shaping and managing the propagation of electromagnetic waves, RISs are primarily utilized to improve signal quality [11, 12], enhance channel capacity [13], mitigate inter-user interference [14] and ensure physical layer security [15].

Despite their potential, RIS-assisted systems inherently experience multiplicative path attenuation and passive RIS, equipped with reflective elements that can solely manipulate the phases of the incident signals, struggles to overcome this hurdle [16, 17]. To address this challenge, the concept of active RIS, capable of simultaneously controlling the magnitudes and phases of incident signals, has been proposed [16, 18–20]. This approach involves integrating active RIS elements with low-power reflective-type amplifiers, such as tunneling reflection amplifiers [21] and amplifying reflect arrays [22]. While this integration allows for the adjustment of the magnitudes of incident waves, it comes with the trade-off of an increase in power consumption and the unavoidable introduction of thermal noise. Specifically, the reflection coefficient of an active RIS element,  $\Omega_a$ , and a passive RIS element,  $\Omega_p$ , can be defined as

$$\Omega_a = \xi_a e^{j\phi_a} \text{ for } \xi_a > 1, \text{ and } \phi_a \in [-\pi, \pi] \quad (1)$$

$$\Omega_p = \xi_p e^{j\phi_p} \text{ for } \xi_p \leq 1, \text{ and } \phi_p \in [-\pi, \pi] \quad (2)$$

where  $|\xi_i|$  and  $\phi_i$  respectively are the magnitude and phase of the corresponding RIS element for  $i \in \{a, p\}$ .

On the other hand, unlike aforementioned RIS architectures, which offer half-space ( $180^\circ$ ) coverage and constrain the transmitter and receiver(s) to be located on the same side of the RIS

[14], simultaneous transmission and reflection RIS (STAR-RIS) concept has been proposed to extend the RIS coverage [23]. This is achieved by enabling simultaneous reflection and transmission of the incident signal, offering further flexibility in the deployment of transmitter and receiver(s) [23]. In STAR-RIS, each of the STAR-RIS element splits the incoming signal from BS in two parts: one part of the signal is reflected on the same side of the incident signal (reflection side), while the second part is transmitted to the opposite side of the incident signal (transmission side) [23]. Therefore, the transmission and reflection coefficients of the STAR-RIS can be modeled as  $\Omega_t = \xi_t e^{j\phi_t}$  and  $\Omega_r = \xi_r e^{j\phi_r}$ , respectively. It is worth noting that controlling transmission and reflection using either a shared or separate reflection-type amplifier in each STAR-RIS element results in either coupled or independent transmission and reflection coefficients [24].

#### A. Prior Works

Recent studies indicate a growing interest in deploying RIS for sensing applications [25–27] that mostly focus on sensing performance [28] and beamforming optimization [29, 30] of RIS-assisted single-target ISAC systems. Although traditional reflection-only passive RISs can improve communication and sensing performance of ISAC systems in challenging non-line-of-sight (NLOS) conditions [26, 27], they struggle to mitigate multiplicative path attenuation due to multi-hop transmission of the sensing link. This limitation restricts their deployment to locations near the transmitter and/or receiver to achieve noticeable performance gains [18]. To overcome this limitation and enhance performance of sensing link, active RIS-assisted ISAC systems, which incorporates additional power amplifiers to modify not only the phase but also the magnitude of an incident electromagnetic wave, has been proposed [31, 32].

More recently, STAR-RIS-assisted ISAC systems have been introduced to achieve full-space coverage and enable flexible deployment of base-stations (BSs), sensing targets, and communication users, independent of their positioning relative to the RIS [33–36]. In [33], a single-target, multi-user ISAC system is proposed, utilizing a STAR-RIS equipping a portion of the surface with one-side sensing-capable elements dedicated to serving sensing targets, while passive transmissive elements are employed to cater to communication users. In [35], a STAR-RIS is placed on the exterior of the vehicle to improve communication for user inside the vehicle while also enabling the vehicle to be tracked and sensed by nearby roadside units (RSUs). A multi-target multi-user ISAC scenario deploying a STAR-RIS with bi-directional sensing elements is presented in [34]. In addition, in [36], receive antennas are positioned on both sides of the STAR-RIS to mitigate severe path attenuation, enabling multi-target multi-user ISAC transmissions on both sides of the STAR-RIS.

#### B. Motivation and Contributions

Motivated by the aforementioned studies, to further improve communication and sensing performance, as well as energy

efficiency of RIS-assisted ISAC systems while achieving full-space coverage, this paper proposes a novel multi-target multi-user ISAC transmission system, utilizing a dual-sided STAR-RIS, with each side offering both reflective and transmissive capabilities. In the proposed scheme, to address severe signal power degradation due to multi-hop transmission, a hybrid STAR-RIS with active transmissive and passive reflective elements is utilized. Unlike [33, 34] that employ sensing capable elements and additional receive antennas [36], leading hardware and implementation complexity, the proposed scheme enables an efficient multi-target multi-user transmission on both sides of STAR-RIS with a more cost-effective and power efficient manner. Moreover, to optimize the transmissive/reflective coefficients of the hybrid STAR-RIS, a non-convex optimization problem is formulated, which is solved via a semi-definite relaxation (SDR)-based approach implemented through CVX toolbox [37]. Furthermore, comprehensive simulations are conducted to evaluate signal-to-interference-noise ratio (SINR) of the communication users and sensing targets and Cramer-Rao bound (CRB) to estimate two-dimensional (2D) angles of departure (AoDs) of the sensing targets. The main contribution of the paper can be summarized as follows:

- In this paper, a hybrid STAR-RIS-enabled ISAC system is introduced to enhance both communication and sensing performance. Unlike [33] and [35] that partition the entire space into distinct sensing and communication regions, the proposed system enables simultaneous sensing and communication in both sides of the STAR-RIS.
- To address the significant path attenuation experienced during multi-hop echo sensing signal transmission in RIS-assisted ISAC systems, the proposed system employs a novel approach compared to those presented in [24, 33, 34, 36, 38], which either use fully active RIS elements [24, 38], allocate a portion of the RIS for sensing-capable elements [33, 34] or leverage a bistatic radar setup with additional receive antennas on both sides of the STAR-RIS [36]. Instead, our system utilizes a dual-sided hybrid STAR-RIS model that incorporates both passive reflective and active transmissive elements, with active transmissive elements amplifying the attenuated signal across multi-hop transmission paths.
- We derive communication and sensing SINR of the proposed scheme. Subsequently, we formulate an optimization problem that maximizes the minimum target SINR by jointly optimizing the reflection and transmission coefficients of the hybrid STAR-RIS under communication SINR constraints. Although enabling multi-user, multi-target transmission on both sides of the STAR-RIS via incorporating both passive reflective and active transmissive elements poses substantial challenges, we reformulate a non-convex optimization problem as a quadratically constrained quadratic programming (QCQP) problem. Then, this non-convex problem is efficiently solved using a semi-definite relaxation (SDR) solution. Moreover, we derive the CRB for estimating the 2D angles of departure (AoDs) of the targets.

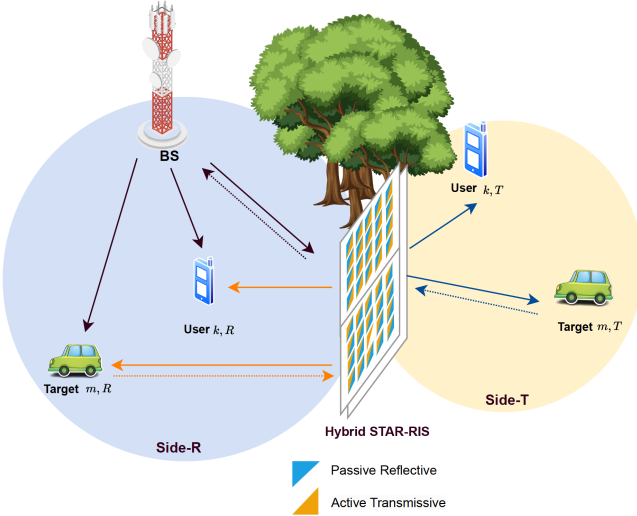


Fig. 1. System model of hybrid RIS-assisted ISAC.

- Thorough performance analyses are conducted via computer simulations to investigate the sensing and communication performance, as well as the power consumption of the proposed system. Moreover, the effectiveness of the hybrid STAR-RIS-aided ISAC system is demonstrated in comparison to benchmark passive STAR-RIS-aided ISAC system.

### C. Organization

The rest of the paper is organized as follows. In Section II, the proposed system model is introduced. Section III provides derivations for sensing performance metrics including target SINR and CRB for 2D AoDs estimation, followed by the proposed optimization algorithm. In Section IV, the numerical results are presented, and this paper concludes with Section V.

*Notation:* Throughout this paper, vectors and matrices are denoted by bold-face lower letter and bold-face upper letter, respectively.  $\mathbb{C}^{K \times L}$  represents the space of a complex matrix with dimensions  $K \times L$ .  $|x|$  stands for absolute value of scalar  $x$ , while  $\|\mathbf{X}\|$  is the Frobenious norm of matrix  $\mathbf{X}$ .  $\mathbf{X}^{-1}$ ,  $\mathbf{X}^T$  and  $\mathbf{X}^H$  represent inverse, transposition and Hermitian of the matrix  $\mathbf{X}$ , respectively. For  $\mathbf{x}$  being a vector,  $\text{diag}(\mathbf{x})$  stands for a diagonal matrix whose diagonal elements are equal to elements of the vector  $\mathbf{x}$ .  $\text{vec}(\mathbf{X})$  is vectorizing operation,  $\text{rect}(\cdot)$  is rectangular function,  $\text{Tr}(\mathbf{X})$  is trace value, and  $\odot$  is Hadamard product.  $\mathbf{I}$  denotes identity matrix, while  $\mathbf{1}$  stands for a vector with all-ones elements.  $\Re(\cdot)$  and  $\Im(\cdot)$  represents real and imaginary components of a complex number, respectively.  $\mathcal{CN}(\mu, \sigma^2)$  denotes distribution of a complex Gaussian random variable with mean  $\mu$  and variance  $\sigma^2$ , and  $\mathcal{O}$  denotes big-O notation.

## II. SYSTEM MODEL

In this section, system model for the proposed hybrid STAR-RIS-enabled ISAC is presented.

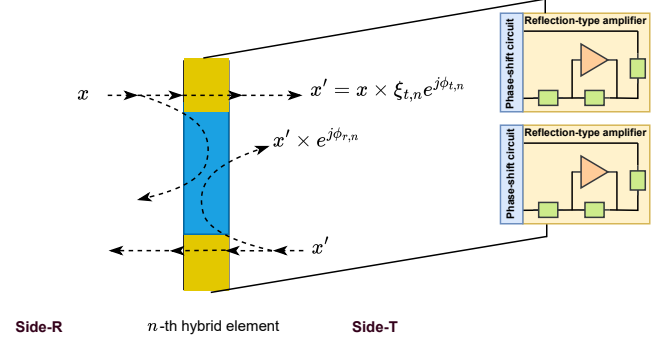


Fig. 2. A generic signal model of the hybrid STAR-RIS.

### A. Hybrid STAR-RIS-Enabled ISAC

The system model of the proposed hybrid STAR-RIS-assisted ISAC is illustrated in Fig. 1. In the proposed system, a uniform linear array (ULA) BS with  $T_x$  antennas communicates with  $K$  single-antenna users, while simultaneously performing  $M$  point targets detection.<sup>1</sup> It is assumed that the coverage space of the BS is split into two parts: transmission (Side-T) and reflection (Side-R) by a hybrid STAR-RIS with a uniform planar array (UPA) consisting  $N$  transmissive/reflective elements. To enable two-side target detection and alleviate path attenuation, the hybrid STAR-RIS operates as a dual-sided STAR-RIS, with “STAR” functionality present on both sides [24, 40], incorporating passive reflective and active transmissive elements. Alternatively, it can be constructed using two adjacent conventional STAR-RIS units oriented oppositely, each featuring active transmissive and passive reflective elements. However, in this paper, for the simplicity of presentation, a dual-sided STAR-RIS with unit-gain passive reflective ( $\xi_{r,n} = 1$ ) and active transmissive elements ( $\xi_{t,n} > 1$ ) is considered, where  $n \in \{1, 2, \dots, N\}$ . Please note that, in the proposed scheme, to independently adjust transmissive and reflection coefficients of the proposed hybrid STAR-RIS, it is assumed that two separate reflection type amplifiers are employed. Then, the amplifiers are assumed to be configured so that on both sides, reflection coefficients maintain unity power ( $\xi_{r,n} = 1$ ) while the transmission amplifier provides an amplification effect ( $\xi_{t,n} > 1$ ) [24]. As a result, the reflection component operates in a passive mode, whereas the transmission component functions in an active mode.

To better illustrate, Fig. 2 presents the signal behaviour of the hybrid STAR-RIS. An incident signal on Side-R, denoted as  $x$ , interacts with the  $n$ -th hybrid element, reflecting with a phase shift  $e^{j\phi_{r,n}}$  as  $x \times e^{j\phi_{r,n}}$  while simultaneously being transmitted toward Side-T through an active transmissive element, resulting in  $x' = x \times \xi_{t,n} e^{j\phi_{t,n}}$ . Similarly, the arriving signal on Side-T, represented as  $x'$ , is reflected as  $x' \times e^{j\phi_{r,n}}$  and transmitted back to Side-R through the active transmissive element, yielding  $x' \times \xi_{t,n} e^{j\phi_{t,n}}$ .

<sup>1</sup>It is assumed that the transceiver operates in full-duplex mode to suppress self interference between joint signal transmission and echo signal reception [39].

Consequently, the transmission and reflection coefficients of the hybrid STAR-RIS with  $N$  elements in both directions can be defined as:

$$\Phi_t \in \mathbb{C}^{N \times N} = \text{diag}(\xi_{t,1}e^{j\phi_{t,1}}, \xi_{t,2}e^{j\phi_{t,2}}, \dots, \xi_{t,N}e^{j\phi_{t,N}}) \quad (3)$$

$$\Phi_r \in \mathbb{C}^{N \times N} = \text{diag}(e^{j\phi_{r,1}}, e^{j\phi_{r,2}}, \dots, e^{j\phi_{r,N}}) \quad (4)$$

where  $\Phi_t$  and  $\Phi_r$  are the transmission and reflection matrices, respectively.

In the proposed scheme, it is assumed that  $K_R$  users and  $M_R$  targets at Side- $R$  receive both direct signals from the BS and indirect signals reflected by the hybrid STAR-RIS, while  $K_T$  users and  $M_T$  targets at Side- $T$  experience obstructed direct links from the BS and can only perceive transmitted signals through the hybrid STAR-RIS, where  $K = K_R + K_T$  and  $M = M_R + M_T$ . It is important to note that throughout the paper, regardless of their distances from the BS, the communication users and sensing targets on Side- $R$  who are located within the same region as the BS are classified as “local”, whereas those on Side- $T$  are referred as “distant”.

In the proposed scheme, to enable simultaneous communication and sensing, the BS transmits following joint signal at  $l$ th time instance, represented by  $\mathbf{x}(l) \in \mathbb{C}^{T_x \times 1}$  becomes

$$\mathbf{x}(l) = \sum_{p=1}^K \mathbf{w}_{c,p} c_p(l) + \sum_{q=1}^M \mathbf{w}_{s,q} s_q(l) \quad (5)$$

$$= \mathbf{W} \tilde{\mathbf{x}}(l) \quad (6)$$

where  $\mathbf{W} \in \mathbb{C}^{T_x \times (K+M)}$  is the overall beamforming matrix. Here,  $c_p(l)$  and  $s_q(l)$  are transmit signals for  $p$ th communication user and  $q$ th sensing target, while  $\mathbf{w}_{c,p} \in \mathbb{C}^{T_x \times 1}$  and  $\mathbf{w}_{s,q} \in \mathbb{C}^{T_x \times 1}$  are their corresponding beamforming vectors, respectively. Therefore, the covariance matrix of the transmit signal can be defined as

$$\mathbf{R}_x = \mathbb{E} \{ \mathbf{x}(l) \mathbf{x}^H(l) \} \quad (7)$$

and maximum transmit power at the BS can be calculated as

$$\begin{aligned} P_{BS} &\geq \sum_{p=1}^K \mathbf{w}_{c,p}^H \mathbf{w}_{c,p} + \sum_{q=1}^M \mathbf{w}_{s,q}^H \mathbf{w}_{s,q} \\ &\geq \text{Tr}(\mathbf{R}_x). \end{aligned} \quad (8)$$

In the proposed scheme, communication signals are generated as complex Gaussian random variables with zero mean and unit variance, i.e.,  $\mathbb{E} \{ \mathbf{c}(l) \mathbf{c}^H(l) \} = \mathbf{I}_K$ , while sensing signals are generated as frequency modulated continuous wave (FMCW) signals [41] as follows

$$s_q(l) = \sum_{\tau=1}^{L_c} A_\tau \text{rect} \left( \frac{l - (\tau - \frac{1}{2}T_c)}{T_c} \right) \cos \left( 2\pi f_c l + \pi \frac{B_w}{L} l^2 \right) \quad (9)$$

where  $L_c$  is the number of chips,  $L$  is the chirp length,  $T_c = L/L_c$  is the chip duration, the  $A_\tau$  is the amplitude of the signal at the  $\tau$ -th time block,  $A_\tau \in \{-1, 1\}$ ,  $f_c$  is the carrier frequency and  $B_w$  is the bandwidth. Moreover, it is assumed that communication and sensing signals are mutually uncorrelated i.e.,  $\mathbb{E} \{ \mathbf{c}(l) \mathbf{s}(l)^H \} = \mathbf{0}_{K \times M}$ .

## B. Communication Model

In the proposed system, all communication channels are modeled by Rician fading channels, and the channels between BS-STAR-RIS (BS-RIS), BS-User  $k$  at Side- $R$  (BS- $\mathbf{U}_{k,R}$ ) and STAR-RIS-User  $k$  at Side  $i$  (RIS- $\mathbf{U}_{k,i}$ ) are respectively represented by  $\mathbf{G} \in \mathbb{C}^{N \times T_x}$ ,  $\mathbf{g}_{k,R} \in \mathbb{C}^{1 \times T_x}$  and  $\mathbf{h}_{k,i} \in \mathbb{C}^{1 \times N}$ , where  $i \in \mathcal{S} = \{T, R\}$  and  $k \in \{1, \dots, K_i\}$ . Here, to simplify the presentation, a unified notation  $\mathbf{D}_c$  is introduced, which can represent  $\mathbf{D}_c \in \{\mathbf{G}, \mathbf{g}_{k,R}, \mathbf{h}_{k,i}\}$ , as follows:

$$\mathbf{D}_c = \sqrt{\alpha_c} \left( \sqrt{\frac{\kappa}{1+\kappa}} \mathbf{D}_c^{\text{LOS}} + \sqrt{\frac{1}{1+\kappa}} \mathbf{D}_c^{\text{NLOS}} \right) \quad (10)$$

where  $\mathbf{D}_c^{\text{LOS}}$  represents the LOS component,  $\mathbf{D}_c^{\text{NLOS}}$  stands for the NLOS component,  $\kappa$  is the Rician factor and  $\alpha_c = \alpha_0 d_c^{-\rho} \in \{\alpha_{\text{BS-RIS}}, \alpha_{\text{BS-}\mathbf{U}_{k,R}}, \alpha_{\text{RIS-}\mathbf{U}_{k,i}}\}$  denotes corresponding path attenuation, for  $\alpha_0$  being the reference path loss at 1 meter (m),  $\rho$  being path-loss exponent and  $d_c \in \{d_{\text{BS-RIS}}, d_{\text{BS-}\mathbf{U}_{k,R}}, d_{\text{RIS-}\mathbf{U}_{k,i}}\}$  being the corresponding distance. Here, each element of  $\mathbf{D}_c^{\text{NLOS}}$  component is assumed to be generated by independent and identically distributed (i.i.d.) complex Gaussian random variables following  $\mathcal{CN}(0, 1)$  distribution, while  $\mathbf{D}_c^{\text{LOS}}$  component is deterministic channel generated by steering vectors. Therefore, the overall  $\mathbf{D}_c$  channel follows  $\mathcal{CN}(\sqrt{\alpha_c} \sqrt{\frac{\kappa}{1+\kappa}} \mathbf{D}_c^{\text{LOS}}, \alpha_c \frac{1}{1+\kappa} \mathbf{I})$ .

Using steering vectors, the LOS component  $\mathbf{G}^{\text{LOS}} \in \mathbb{C}^{N \times T_x}$  of the channel between BS-STAR-RIS is generated as:

$$\mathbf{G}^{\text{LOS}} = \mathbf{b}^H(\varphi_{c,h}^{\text{RIS}}, \varphi_{c,v}^{\text{RIS}}) \mathbf{a}(\theta_{c,h}^{\text{RIS}}, \theta_{c,v}^{\text{RIS}}) \quad (11)$$

where  $\mathbf{a}(\theta_{c,h}^{\text{RIS}}, \theta_{c,v}^{\text{RIS}}) \in \mathbb{C}^{1 \times T_x}$  and  $\mathbf{b}(\varphi_{c,h}^{\text{RIS}}, \varphi_{c,v}^{\text{RIS}}) \in \mathbb{C}^{1 \times N}$  are the ULA and UPA array factors of BS and hybrid STAR-RIS, respectively. Here,  $N = N_x \times N_y$  with  $N_x$  and  $N_y$  representing the number of hybrid STAR-RIS elements located horizontally and vertically on  $x$ - $y$  plane, respectively.  $\theta_{c,h}^{\text{RIS}}, \theta_{c,v}^{\text{RIS}}$  are horizontal and vertical AoDs from BS towards RIS, while  $\varphi_{c,h}^{\text{RIS}}, \varphi_{c,v}^{\text{RIS}}$  are the horizontal, vertical angles of arrival (AoA) at RIS, respectively. Here,  $\mathbf{a}(\theta_{c,h}^{\text{RIS}}, \theta_{c,v}^{\text{RIS}})$  and  $\mathbf{b}(\varphi_{c,h}^{\text{RIS}}, \varphi_{c,v}^{\text{RIS}})$  array factors are given as

$$\mathbf{a}(\theta_{c,h}^{\text{RIS}}, \theta_{c,v}^{\text{RIS}}) = [1, \dots, e^{j\eta_{BS}(T_x-1) \sin(\theta_{c,h}^{\text{RIS}}) \cos(\theta_{c,v}^{\text{RIS}})}] \quad (12)$$

$$\mathbf{b}(\varphi_{c,h}^{\text{RIS}}, \varphi_{c,v}^{\text{RIS}}) = \mathbf{b}^x(\varphi_{c,h}^{\text{RIS}}, \varphi_{c,v}^{\text{RIS}}) \otimes \mathbf{b}^y(\varphi_{c,h}^{\text{RIS}}, \varphi_{c,v}^{\text{RIS}}) \quad (13)$$

where  $\eta_{BS} = \frac{2\pi}{\lambda} d_{BS}$  for  $\lambda$  wavelength and  $d_{BS}$  distance between two adjacent transmit/receive antennas at BS, respectively. Here,  $\mathbf{b}^x(\varphi_{c,h}^{\text{RIS}}, \varphi_{c,v}^{\text{RIS}}) \in \mathbb{C}^{1 \times N_x}$  and  $\mathbf{b}^y(\varphi_{c,h}^{\text{RIS}}, \varphi_{c,v}^{\text{RIS}}) \in \mathbb{C}^{1 \times N_y}$  are respectively steering vectors of STAR-RIS in  $x$  and  $y$  dimensions given as

$$\mathbf{b}^x(\varphi_{c,h}^{\text{RIS}}, \varphi_{c,v}^{\text{RIS}}) = [1, \dots, e^{j\eta_{RIS}(N_x-1) \sin(\varphi_{c,h}^{\text{RIS}}) \cos(\varphi_{c,v}^{\text{RIS}})}] \quad (14)$$

$$\mathbf{b}^y(\varphi_{c,h}^{\text{RIS}}, \varphi_{c,v}^{\text{RIS}}) = [1, \dots, e^{j\eta_{RIS}(N_y-1) \sin(\varphi_{c,h}^{\text{RIS}}) \sin(\varphi_{c,v}^{\text{RIS}})}] \quad (15)$$

where  $\eta_{RIS} = \frac{2\pi}{\lambda} d_{RIS}$  for  $d_{RIS}$  being horizontal and vertical distance between two adjacent elements at STAR-RIS. Therefore, (13) can be simply rewritten as

$$\mathbf{b}(\varphi_{c,h}^{\text{RIS}}, \varphi_{c,v}^{\text{RIS}}) = e^{j\eta_{RIS} \mathbf{k}(\varphi_{c,h}^{\text{RIS}}, \varphi_{c,v}^{\text{RIS}})} \quad (16)$$

where  $\mathbf{k}(\varphi_{c,h}^{\text{RIS}}, \varphi_{c,v}^{\text{RIS}}) \in \mathbb{C}^{1 \times N} = \mathbf{k}_x \sin(\varphi_{c,h}^{\text{RIS}}) \cos(\varphi_{c,v}^{\text{RIS}}) + \mathbf{k}_y \sin(\varphi_{c,h}^{\text{RIS}}) \sin(\varphi_{c,v}^{\text{RIS}})$ . Here,  $\mathbf{k}_x \in \mathbb{C}^{1 \times N} = \mathbf{e}_x \otimes \mathbf{1}_{N_y}$  and  $\mathbf{k}_y \in \mathbb{C}^{1 \times N} = \mathbf{1}_{N_x} \otimes \mathbf{e}_y$  are with scalar components for  $\mathbf{e}_x \in \mathbb{C}^{1 \times N_x} = [0, 1, \dots, N_x-1]$  and  $\mathbf{e}_y \in \mathbb{C}^{1 \times N_y} = [0, 1, \dots, N_y-1]$ .

Similarly, the LOS channel components of the channel between BS- $U_{k,R}$  and RIS- $U_{k,i}$  can be generated as  $\mathbf{g}_{k,R}^{\text{LOS}} = \mathbf{a}(\theta_{c,h}^{k,R}, \theta_{c,v}^{k,R}) \in \mathbb{C}^{1 \times T_x}$  and  $\mathbf{h}_{k,i}^{\text{LOS}} = \mathbf{b}(\varphi_{c,h}^{k,i}, \varphi_{c,v}^{k,i}) \in \mathbb{C}^{1 \times N}$ , where  $\{\theta_{c,h}^{k,R}, \theta_{c,v}^{k,R}\}$  and  $\{\varphi_{c,h}^{k,i}, \varphi_{c,v}^{k,i}\}$  are horizontal and vertical AoD pairs from the BS towards  $U_{k,R}$  and from STAR-RIS towards  $U_{k,i}$  at Side  $i \in \mathcal{S} = \{T, R\}$ , respectively. Then, following ULA and UPA in (12) and (16)  $\mathbf{a}(\theta_{c,h}^{k,R}, \theta_{c,v}^{k,R})$  and  $\mathbf{b}(\varphi_{c,h}^{k,i}, \varphi_{c,v}^{k,i})$  can be given as

$$\mathbf{a}(\theta_{c,h}^{k,R}, \theta_{c,v}^{k,R}) = [1, \dots, e^{j\eta_{\text{BS}}(T_x-1)\sin(\theta_{c,h}^{k,R})\cos(\theta_{c,v}^{k,R})}] \quad (17)$$

$$\mathbf{b}(\varphi_{c,h}^{k,i}, \varphi_{c,v}^{k,i}) = e^{j\eta_{\text{RIS}}\mathbf{k}(\varphi_{c,h}^{k,i}, \varphi_{c,v}^{k,i})} \quad (18)$$

where  $\mathbf{k}(\varphi_{c,h}^{k,i}, \varphi_{c,v}^{k,i}) \in \mathbb{C}^{1 \times N} = \mathbf{k}_x \sin(\varphi_{c,h}^{k,i}) \cos(\varphi_{c,v}^{k,i}) + \mathbf{k}_y \sin(\varphi_{c,h}^{k,i}) \sin(\varphi_{c,v}^{k,i})$ . Then, following (5) and (10), the received signal at  $U_{k,T}$  that perceives the transmit signals from the BS over the active transmissive elements of the hybrid STAR-RIS becomes

$$\begin{aligned} y_c^{k,T}(l) &= \mathbf{h}_{k,T} \Phi_t \mathbf{G} \mathbf{w}_{c,k} c_k(l) + \underbrace{\sum_{q=1}^M \mathbf{h}_{k,T} \Phi_t \mathbf{G} \mathbf{w}_{s,q} s_q(l)}_{\text{sensing interference}} \\ &+ \underbrace{\sum_{\tilde{k} \neq k} \mathbf{h}_{k,T} \Phi_t \mathbf{G} \mathbf{w}_{c,\tilde{k}} \tilde{c}_{\tilde{k}}(l)}_{\text{user interference}} + \underbrace{\sum_{\tilde{k}=K_T+1}^K \mathbf{h}_{k,T} \Phi_t \mathbf{G} \mathbf{w}_{c,\tilde{k}} \tilde{c}_{\tilde{k}}(l)}_{\text{thermal noise}} + \underbrace{n_c^{k,T}(l)}_{\text{static noise}} \end{aligned} \quad (19)$$

where  $n_c^{k,T}(l) \in \mathcal{CN}(0, \sigma_{n_c}^2)$  is the static additive white Gaussian noise (AWGN) sample and  $\mathbf{v}_1 \in \mathbb{C}^{N \times 1}$  is the non-negligible internal thermal noise introduced by reflection-type amplifiers of active STAR-RIS elements [19] whose each element is i.i.d. and follows  $\mathcal{CN}(0, \sigma_{v_1}^2)$  for  $k \in \{1, \dots, K_T\}$  and  $\tilde{k} \in \{1, \dots, K\}$ .

Likewise, for the communication users at Side- $R$  that receive signals from BS through the direct path and reflected path over passive reflective elements of the hybrid STAR-RIS, the received signal at  $U_{k,R}$  can be given as

$$\begin{aligned} y_c^{k,R}(l) &= \bar{\mathbf{h}}_{k,R} \mathbf{w}_{c,k} c_k(l) + \sum_{\tilde{k} \neq k} \bar{\mathbf{h}}_{k,R} \mathbf{w}_{c,\tilde{k}} \tilde{c}_{\tilde{k}}(l) + \sum_{\tilde{k}=K_R+1}^K \bar{\mathbf{h}}_{k,R} \mathbf{w}_{c,\tilde{k}} \tilde{c}_{\tilde{k}}(l) \\ &+ \sum_{q=1}^M \bar{\mathbf{h}}_{k,R} \mathbf{w}_{s,q} s_q(l) + n_c^{k,R}(l) \end{aligned} \quad (20)$$

where  $\bar{\mathbf{h}}_{k,R} = \mathbf{h}_{k,R} \Phi_r \mathbf{G} + \mathbf{g}_{k,R}$  and  $n_c^{k,R}(l) \sim \mathcal{CN}(0, \sigma_{n_c}^2)$  is the overall noise figure between the BS and  $U_{k,R}$  for  $k \in \{1, \dots, K_R\}$  and  $\tilde{k} \in \{1, \dots, K\}$ .

### C. Sensing Model

In the proposed system, the paths from the BS and hybrid STAR-RIS towards the targets are deterministic channels and constructed using steering vectors. The channel between the STAR-RIS and the target  $m$  at Side- $i$  ( $O_{m,i}$ ) can be given in terms of the AoD pair of  $\{\varphi_{s,h}^{m,i}, \varphi_{s,v}^{m,i}\}$  as follows

$$\mathbf{b}(\varphi_{s,h}^{m,i}, \varphi_{s,v}^{m,i}) = e^{j\eta_{\text{RIS}}\mathbf{k}(\varphi_{s,h}^{m,i}, \varphi_{s,v}^{m,i})} \quad (21)$$

where  $\mathbf{b}(\varphi_{s,h}^{m,i}, \varphi_{s,v}^{m,i}) \in \mathbb{C}^{1 \times N}$ ,  $\mathbf{k}(\varphi_{s,h}^{m,i}, \varphi_{s,v}^{m,i}) \in \mathbb{C}^{1 \times N} = \mathbf{k}_x \sin(\varphi_{s,h}^{m,i}) \cos(\varphi_{s,v}^{m,i}) + \mathbf{k}_y \sin(\varphi_{s,h}^{m,i}) \sin(\varphi_{s,v}^{m,i})$ . Thus, the re-

ceived echo signal at the BS from the  $m$ th sensing target on Side- $T$  ( $O_{m,T}$ ) follows the path of BS  $\rightarrow$  STAR-RIS  $\rightarrow O_{m,T} \rightarrow$  STAR-RIS  $\rightarrow$  BS. In order to mitigate severe path attenuation due to this multi-hop transmission, the considered dual-sided hybrid STAR-RIS utilizes active elements in transmission mode in both directions. Then, the received echo signal collected at the BS due to the sensing target  $O_{m,T}$  becomes

$$\mathbf{y}_s^{m,T}(l) = \beta_{\text{RIS}}^{m,T} \mathbf{G}^H \Phi_t^H \mathbf{B}_m \Phi_t \mathbf{G} \mathbf{x}(l) + \tilde{\mathbf{n}}_s^{m,T}(l) \quad (22)$$

where  $m \in \{1, \dots, M_T\}$ ,  $\beta_{\text{RIS}}^{m,T}$  is the round-trip path attenuation,  $\mathbf{B}_m = \mathbf{b}^H(\varphi_{s,h}^{m,T}, \varphi_{s,v}^{m,T}) \mathbf{b}(\varphi_{s,h}^{m,T}, \varphi_{s,v}^{m,T})$ ,  $\tilde{\mathbf{n}}_s^{m,T}(l) = \mathbf{G}^H \Phi_t^H \mathbf{B}_m \Phi_t \mathbf{v}_1(l) + \mathbf{G}^H \Phi_t^H \mathbf{v}_2(l) + \mathbf{n}_s^{m,T}(l)$  is the overall noise samples vector including thermal noise of active transmissive elements and static noise in the channel for  $\mathbf{n}_s^{m,T}(l)$  being static noise and following  $\sim \mathcal{CN}(0, \sigma_{n_s}^2 \mathbf{I})$  distribution, while  $\mathbf{v}_1(l)$  and  $\mathbf{v}_2(l)$  are the thermal noise vectors with the  $\mathcal{CN}(0, \sigma_{v_1}^2 \mathbf{I})$  and  $\mathcal{CN}(0, \sigma_{v_2}^2 \mathbf{I})$  distributions, respectively. Here, for the sake of simplicity, the thermal and static noise variances are assumed to be  $\sigma_{n_s}^2 = \sigma_{v,1}^2 = \sigma_{v,2}^2$ . It is important to note that for  $P_A = \sqrt{\text{Tr}(\Phi_t^H \Phi_t)} = \sqrt{\sum_{n=1}^N |\xi_{t,n}|^2}$  being the overall amplification factor of the active transmissive elements, a low  $P_A$  amplification factor implies that the internal thermal noise of the active transmissive STAR-RIS elements remains negligible. This is because the path attenuation terms in the first and second expressions of  $\tilde{\mathbf{n}}_s^{m,T}(l)$  make them insignificant, resulting in  $\tilde{\mathbf{n}}_s^{m,T}(l) \approx \mathbf{n}_s^{m,T}(l)$ . In this case, the distribution of  $\tilde{\mathbf{n}}_s^{m,T}(l)$  approximates to  $\sim \mathcal{CN}(0, \sigma_{n_s}^2 \mathbf{I})$  where  $\sigma_{n_s}^2 = \sigma_{n_s}^2$ . On the other hand, for very high  $P_A$  values, the internal thermal noise effect becomes significant. In that case,  $\tilde{\mathbf{n}}_s^{m,T}(l) \approx \mathbf{G}^H \Phi_t^H \mathbf{B}_m \Phi_t \mathbf{v}_1(l)$ . Thus, the overall noise variance becomes  $\sigma_{n_s}^2 = \sigma_{n_s}^2 |\langle \Psi(n, n) \rangle|^2 \alpha_{\text{BS-RIS}} \left( \frac{\kappa}{1+\kappa} \sum_v |\mathbf{G}^{\text{LOS}}(n, v)|^2 + \frac{1}{1+\kappa} \right)$ , where  $\Psi = \Phi_t^H \mathbf{B}_m \Phi_t$  and  $v \in \{1, 2, \dots, T_x\}$ .

Then, using (22), the overall received echo signal over the  $L$  time block is given as

$$\mathbf{Y}_s^{m,T} = \beta_{\text{RIS}}^{m,T} \mathbf{G}^H \Phi_t^H \mathbf{B}_m \Phi_t \mathbf{G} \mathbf{X} + \tilde{\mathbf{N}}_s^{m,T} \quad (23)$$

where  $\mathbf{Y}_s^{m,T} = [\mathbf{y}_s^{m,T}(1), \dots, \mathbf{y}_s^{m,T}(L)]$ ,  $\mathbf{X} = [\mathbf{x}(1), \dots, \mathbf{x}(L)]$  and  $\tilde{\mathbf{N}}_s^{m,T} = [\tilde{\mathbf{n}}_s^{m,T}(1), \dots, \tilde{\mathbf{n}}_s^{m,T}(L)]$ . In the proposed scheme, the active transmissive STAR-RIS elements are first employed to transmit BS signals to Side- $T$  and then reflect the echo signals of the distant targets back to the BS. Therefore, using (23), the overall power consumption of the active transmissive elements can be calculated as

$$P_{\text{RIS}} \geq \|\Phi_t \mathbf{G} \mathbf{x}(l)\|^2 + \|\Phi_t^H \mathbf{B}_m \Phi_t \mathbf{G} \mathbf{x}(l)\|^2 + \|\Phi_t^H \mathbf{B}_m \Phi_t \mathbf{v}_1(l)\|^2 + \|\Phi_t^H \mathbf{v}_2(l)\|^2. \quad (24)$$

After some manipulations, (24) can be rewritten as

$$\begin{aligned} P_{\text{RIS}} &\geq \text{Tr}(\Phi_t \mathbf{G} \mathbf{R}_x \mathbf{G}^H \Phi_t^H) + \text{Tr}(\Phi_t^H \mathbf{B}_m \Phi_t \mathbf{G} \mathbf{R}_x \mathbf{G}^H \Phi_t^H \mathbf{B}_m \Phi_t) \\ &+ \sigma_{v_1}^2 \text{Tr}(\Phi_t^H \mathbf{B}_m \Phi_t \Phi_t^H \mathbf{B}_m \Phi_t) + \sigma_{v_2}^2 \text{Tr}(\Phi_t^H \Phi_t). \end{aligned} \quad (25)$$

Furthermore, for the mono-static MIMO radar systems

<sup>2</sup>For  $Z = XY$ , where  $X$  and  $Y$  are independent random variables, the distribution of  $Z$  is characterized by  $\mu_Z = \mu_X \mu_Y$  and  $\sigma_Z^2 = \sigma_X^2 \mu_Y^2 + \sigma_Y^2 \mu_X^2 + \mu_X^2 \mu_Y^2$  [42].

$$\gamma_{m,T} \leq \frac{(\beta_{\text{RIS}}^{m,T})^2 \text{Tr}(\bar{\mathbf{G}} \Phi_t \mathbf{B}_m \Phi_t^H) \text{Tr}(\mathbf{R}_x)}{\sum_{j \neq m}^{M_R} \text{Tr}(\mathbf{f}_{j,R}^H \mathbf{f}_{j,R})^2 \text{Tr}(\mathbf{R}_x) + \sum_{\tilde{m} \neq m}^{M_T} (\beta_{\text{RIS}}^{\tilde{m},T})^2 \text{Tr}(\bar{\mathbf{G}} \Phi_t \mathbf{B}_{\tilde{m},T} \Phi_t^H) \text{Tr}(\mathbf{R}_x) + \sigma_{n_s}^2} \quad (31)$$

$$\gamma_{m,T} \leq \frac{(\beta_{\text{RIS}}^{m,T})^2 \text{Tr}(\bar{\mathbf{B}}_{m,T} \Phi_t^H \mathbf{A} \Phi_t) \text{Tr}(\Phi_t \Phi_t^H) \text{Tr}(\mathbf{R}_x)}{\sum_{j \neq m}^{M_R} \text{Tr}(\mathbf{f}_{j,R}^H \mathbf{f}_{j,R})^2 \text{Tr}(\mathbf{R}_x) + \sum_{\tilde{m} \neq m}^{M_T} (\beta_{\text{RIS}}^{\tilde{m},T})^2 \text{Tr}(\bar{\mathbf{B}}_{\tilde{m},T}^H \Phi_t^H \mathbf{A} \Phi_t) \text{Tr}(\Phi_t \Phi_t^H) \text{Tr}(\mathbf{R}_x) + \sigma_{n_s}^2} \quad (32)$$

whose transmit and receive elements are co-located, the round-trip path loss is calculated as [31, 43]

$$\beta = \sqrt{\frac{\lambda^2 \Lambda}{(4\pi)^3 d^4}} \quad (26)$$

where  $\Lambda$  is the radar cross section (RCS) and  $d$  is the distance between MIMO radar and the sensing target. Therefore, in the proposed scenario, since the hybrid STAR-RIS can be considered as a mono-static MIMO radar [31], the path attenuation coefficient of  $\beta_{\text{RIS}}^{m,T}$  in (23) is calculated for the corresponding distance  $d = d_{\text{RIS-O}_{m,T}}$ .

Unlike the distant sensing targets, since the local sensing targets on Side- $R$  have both direct and indirect connections with the BS, similar to (17), the channel between BS and sensing target  $m$  on Side- $R$  ( $\mathbf{O}_{m,R}$ ),  $\mathbf{a}(\theta_{s,h}^{m,R}, \theta_{s,v}^{m,R}) \in \mathbb{C}^{1 \times T_x}$ , can be expressed as

$$\mathbf{a}(\theta_{s,h}^{m,R}, \theta_{s,v}^{m,R}) = [1, \dots, e^{j\eta_{\text{BS}}(T_x-1) \sin(\theta_{s,h}^{m,R}) \cos(\theta_{s,v}^{m,R})}] \quad (27)$$

where  $m \in \{1, \dots, M_R\}$ ,  $\theta_{s,h}^{m,R}$  and  $\theta_{s,v}^{m,R}$  are horizontal and vertical AoDs from BS towards target  $\mathbf{O}_{m,R}$ , respectively. Therefore, following (27) and (21) for  $i = R$ , the received echo signal collected at the BS from the target  $\mathbf{O}_{m,R}$  over the paths of  $\text{BS} \rightarrow \mathbf{O}_{m,R} \rightarrow \text{BS}$  and  $\text{BS} \rightarrow \text{STAR-RIS} \rightarrow \mathbf{O}_{m,R} \rightarrow \text{STAR-RIS} \rightarrow \text{BS}$  becomes [44]

$$\mathbf{y}_s^{m,R}(l) = \beta_{\text{BS}}^{m,R} (\mathbf{a}(\theta_{s,h}^{m,R}, \theta_{s,v}^{m,R}) + \tilde{\mathbf{b}}(\varphi_{s,h}^{m,R}, \varphi_{s,v}^{m,R}) \Phi_r \mathbf{G})^H \times (\mathbf{a}(\theta_{s,h}^{m,R}, \theta_{s,v}^{m,R}) + \tilde{\mathbf{b}}(\varphi_{s,h}^{m,R}, \varphi_{s,v}^{m,R}) \Phi_r \mathbf{G}) \mathbf{x}(l) + \mathbf{n}_s^{m,R}(l) \quad (28)$$

where  $\mathbf{n}_s^{m,R}$  is the AWGN matrix whose each entry is i.i.d and with  $\sim \mathcal{CN}(0, \sigma_{m,R}^2)$  distribution and  $\tilde{\mathbf{b}}(\varphi_{s,h}^{m,R}, \varphi_{s,v}^{m,R}) \in \mathbb{C}^{1 \times N} = \sqrt{\beta_{\text{RIS}}^{m,R} / \beta_{\text{BS}}^{m,R}} \mathbf{b}(\varphi_{s,h}^{m,R}, \varphi_{s,v}^{m,R})$  for  $\beta_{\text{BS}}^{m,R}$  and  $\beta_{\text{RIS}}^{m,R}$  being the round-trip path attenuation from the BS and hybrid STAR-RIS to the target  $\mathbf{O}_{m,R}$  calculated as in (26) for corresponding  $d = d_{\text{BS-O}_{m,R}}$  and  $d = d_{\text{RIS-O}_{m,R}}$ , respectively. Then, over the  $L$  time block, (28) can be rewritten as

$$\mathbf{Y}_s^{m,R} = \beta_{\text{BS}}^{m,R} (\mathbf{a}(\theta_{s,h}^{m,R}, \theta_{s,v}^{m,R}) + \tilde{\mathbf{b}}(\varphi_{s,h}^{m,R}, \varphi_{s,v}^{m,R}) \Phi_r \mathbf{G})^H \times (\mathbf{a}(\theta_{s,h}^{m,R}, \theta_{s,v}^{m,R}) + \tilde{\mathbf{b}}(\varphi_{s,h}^{m,R}, \varphi_{s,v}^{m,R}) \Phi_r \mathbf{G}) \mathbf{X} + \mathbf{N}_s^{m,R} \quad (29)$$

where  $\mathbf{Y}_s^{m,R} = [\mathbf{y}_s^{m,R}(1), \dots, \mathbf{y}_s^{m,R}(L)]$  and  $\mathbf{N}_s^{m,R} = [\mathbf{N}_s^{m,R}(1), \dots, \mathbf{N}_s^{m,R}(L)]$ .

### III. PERFORMANCE METRICS AND PROBLEM FORMULATION

In this section, sensing and communication metrics of the for the proposed system are derived. Subsequently, an optimization problem that maximizes the minimum SINR

of the sensing targets, subject to the communication SINR constraint, is formulated by optimizing transmissive/reflective coefficients of the hybrid STAR-RIS and beamforming matrix. Moreover, the CRB for estimating 2D AoDs of the sensing targets is derived. To effectively solve this optimization, the problem is reformulated into linear and quadratic components, thus enabling the problem to be solved through a SDR-based approach.

#### A. Target SINR Analysis

In this subsection, the performance of the target SINR is determined.

Using (23), for the distant targets on the Side- $T$  that perceive transmit signals through the active transmissive STAR-RIS elements, the target SINR can be given, considering interference from the other sensing targets both on Side- $R$  and Side- $T$ , as

$$\gamma_{m,T} = \frac{\left\| \beta_{\text{RIS}}^{m,T} \mathbf{G}^H \Phi_t^H \mathbf{B}_m \Phi_t \mathbf{G} \mathbf{X} \right\|^2}{\sum_{j=1}^{M_R} \left\| \mathbf{f}_{j,R}^H \mathbf{f}_{j,R} \mathbf{X} \right\|^2 + \sum_{\tilde{m} \neq m}^{M_T} \left\| \beta_{\text{RIS}}^{\tilde{m},T} \mathbf{G}^H \Phi_t^H \mathbf{B}_{\tilde{m},T} \Phi_t \mathbf{G} \mathbf{X} \right\|^2 + \sigma_{n_s}^2} \quad (30)$$

where  $\mathbf{f}_{j,R} = \beta_{\text{BS}}^{j,R} (\mathbf{a}(\theta_{s,h}^{j,R}, \theta_{s,v}^{j,R}) + \tilde{\mathbf{b}}(\varphi_{s,h}^{j,R}, \varphi_{s,v}^{j,R}) \Phi_r \mathbf{G})$ . After some simplification<sup>2</sup>, (30) can be rewritten as in (31) for  $\bar{\mathbf{G}} = \mathbf{G}^H \mathbf{G}$  at the beginning of the this page.

Here, employing Cauchy Schwartz inequality [45] for  $\text{Tr}(\mathbf{K}\mathbf{L})^2 \leq \text{Tr}(\mathbf{K}^H \mathbf{K}) \text{Tr}(\mathbf{L}^H \mathbf{L})$ , the target SINR of  $\mathbf{O}_{m,T}$  in (31) is upper bounded as in (32). Then, using [45, Theorem 1.10], for  $\mathbf{Q}_{m,T} \in \mathbb{C}^{N \times N} = \mathbf{B}_m \mathbf{B}_m^H \odot \bar{\mathbf{G}}^H \bar{\mathbf{G}}$ ,  $\mathbf{Q}_{\tilde{m},T} \in \mathbb{C}^{N \times N} = \mathbf{B}_{\tilde{m}} \mathbf{B}_{\tilde{m}}^H \odot \bar{\mathbf{G}}^H \bar{\mathbf{G}}$  and  $\mathbf{Z}_t \in \mathbb{C}^{N \times N} = \mathbf{z}_t^H \mathbf{z}_t$  for  $\mathbf{z}_t \in \mathbb{C}^{1 \times N} = [\xi_{t,1} e^{j\phi_{t,1}}, \xi_{t,2} e^{j\phi_{t,2}}, \dots, \xi_{t,N} e^{j\phi_{t,N}}]$ , the target SINR in (32) can be bounded as in (33), which appears at the top of the next page.

Similarly, considering the received echo signal given in (29), the SINR of the target  $\mathbf{O}_{m,R}$  can be expressed as

$$\gamma_{m,R} = \frac{\left\| \mathbf{f}_{k,R}^H \mathbf{f}_{k,R} \mathbf{X} \right\|^2}{\sum_{\tilde{m} \neq m}^{M_R} \left\| \mathbf{f}_{m,R}^H \mathbf{f}_{m,R} \mathbf{X} \right\|^2 + \sum_{j=1}^{M_T} \left\| \beta_{\text{RIS}}^{j,T} \mathbf{G}^H \Phi_t^H \mathbf{B}_{j,T} \Phi_t \mathbf{G} \mathbf{X} \right\|^2 + \sigma_{n_s}^2} \quad (34)$$

Therefore, for  $\text{Tr}(\Phi_r^H \Phi_r) = N$  and using  $\text{Tr}((\mathbf{K} + \mathbf{L})(\mathbf{K} + \mathbf{L})^H) \leq 2(\text{Tr}(\mathbf{K}\mathbf{K}^H) + \text{Tr}(\mathbf{L}\mathbf{L}^H))$  [45], the target

<sup>2</sup>For  $\mathbf{K}, \mathbf{L}$  and  $\mathbf{M}$  being matrices with coherent dimensions, the trace of matrix product is  $\text{Tr}(\mathbf{K}\mathbf{L}\mathbf{M}) = \text{Tr}(\mathbf{M}\mathbf{K}\mathbf{L}) = \text{Tr}(\mathbf{L}\mathbf{M}\mathbf{K})$  [45].

$$\gamma_{m,T} \leq \frac{P_A^2 (\beta_{\text{RIS}}^{m,T})^2 \text{Tr}(\mathbf{Q}_{m,T} \mathbf{Z}_t) \text{Tr}(\mathbf{R}_x)}{\sum_{j \neq m}^{M_R} \text{Tr}((\mathbf{f}_{j,R}^H \mathbf{f}_{j,R})^2) \text{Tr}(\mathbf{R}_x) + \sum_{\tilde{m} \neq m}^{M_T} P_A^2 (\beta_{\text{RIS}}^{\tilde{m},T})^2 \text{Tr}(\mathbf{Q}_{\tilde{m},T} \mathbf{Z}_t) \text{Tr}(\mathbf{R}_x) + \sigma_{\tilde{n}_s}^2} \quad (33)$$

$$\gamma_{m,R} \leq \frac{(\beta_{\text{BS}}^{m,R})^2 \text{Tr}(\mathbf{R}_x) (\text{Tr}(\mathbf{A}_m \mathbf{A}_m^H)^2 + N \text{Tr}(\mathbf{Q}_{m,R} \mathbf{Z}_r))}{\sum_{\tilde{m} \neq m}^{M_R} (\beta_{\text{BS}}^{\tilde{m},R})^2 \text{Tr}(\mathbf{R}_x) ((\text{Tr}(\mathbf{A}_{\tilde{m},R} \mathbf{A}_{\tilde{m},R}^H)^2 + N \text{Tr}(\mathbf{Q}_{\tilde{m},R} \mathbf{Z}_r)) + \sum_{j=1}^{M_T} P_A^2 (\beta_{\text{RIS}}^{j,T})^2 \text{Tr}(\mathbf{Q}_{j,T} \mathbf{Z}_t) \text{Tr}(\mathbf{R}_x) + \sigma_{\tilde{n}_s}^2} \quad (35)$$

SINR of each  $\mathbf{O}_{m,R}$  can be upper bounded as in (35), where  $\mathbf{A}_m \in \mathbb{C}^{T_x \times T_x} = \mathbf{a}(\theta_{s,h}^{m,R}, \theta_{s,v}^{m,R}) \mathbf{a}^H(\theta_{s,h}^{m,R}, \theta_{s,v}^{m,R})$ ,  $\mathbf{Q}_{m,R} \in \mathbb{C}^{N \times N} = \tilde{\mathbf{B}}_m \tilde{\mathbf{B}}_m^H \odot \tilde{\mathbf{G}}^H \tilde{\mathbf{G}}$ ,  $\tilde{\mathbf{B}}_m \in \mathbb{C}^{N \times N} = \tilde{\mathbf{b}}(\varphi_{s,h}^{m,R}, \varphi_{s,v}^{m,R})^H \tilde{\mathbf{b}}(\varphi_{s,h}^{m,R}, \varphi_{s,v}^{m,R})$ ,  $\mathbf{Z}_r \in \mathbb{C}^{N \times N} = \mathbf{z}_r^H \mathbf{z}_r$ ,  $\mathbf{z}_r \in \mathbb{C}^{1 \times N} = [e^{j\phi_{r,1}}, e^{j\phi_{r,2}}, \dots, e^{j\phi_{r,N}}]$  and  $j \in \{1, \dots, M_T\}$ .

### B. User SINR Analysis

In this subsection, the SINR of the communication users is derived.

Using (19), the SINR of user  $\mathbf{U}_{k,T}$  can be simply given as

$$R_{k,T} = \frac{|\mathbf{h}_{k,T} \Phi_t \mathbf{G} \mathbf{w}_{c,k}|^2}{\sum_{\tilde{k} \neq k}^{K_T} |\mathbf{h}_{k,T} \Phi_t \mathbf{G} \mathbf{w}_{c,\tilde{k}}|^2 + \sum_{\tilde{k}=K_T+1}^K |\mathbf{h}_{k,T} \Phi_t \mathbf{G} \mathbf{w}_{c,\tilde{k}}|^2 + \sum_{q=1}^M |\mathbf{h}_{k,T} \Phi_t \mathbf{G} \mathbf{w}_{s,q}|^2 + \sigma_{\tilde{n}_c}^2} \quad (36)$$

where  $\sigma_{\tilde{n}_c}^2$  is the variance of the overall noise figure  $\tilde{n}_c^{k,T}$  of the user  $\mathbf{U}_{k,T}$  which is calculated as  $\sigma_{\tilde{n}_c}^2 = P_A^2 \alpha_{\text{RIS-U}_{k,T}} (\frac{\kappa}{1+\kappa} \|\mathbf{h}_{k,T}^{\text{LOS}}\|^2 + \frac{1}{1+\kappa})$ . Here, using above matrix conversions [45], for  $\mathbf{V}_{k,T} = \mathbf{h}_{k,T}^H \mathbf{h}_{k,T} \odot (\mathbf{G} \mathbf{w}_{c,k})(\mathbf{G} \mathbf{w}_{c,k})^H$ ,  $\mathbf{V}_{\tilde{k},T} = \mathbf{h}_{\tilde{k},T}^H \mathbf{h}_{\tilde{k},T} \odot (\mathbf{G} \mathbf{w}_{c,\tilde{k}})(\mathbf{G} \mathbf{w}_{c,\tilde{k}})^H$  and  $\mathbf{V}_{q,T} = \mathbf{h}_{k,T}^H \mathbf{h}_{k,T} \odot (\mathbf{G} \mathbf{w}_{c,q})(\mathbf{G} \mathbf{w}_{c,q})^H$ , (36) can be rewritten in a simplified form as

$$R_{k,T} = \frac{\text{Tr}(\mathbf{V}_{k,T} \mathbf{Z}_t)}{\sum_{\tilde{k} \neq k}^{K_T} \text{Tr}(\mathbf{V}_{\tilde{k},T} \mathbf{Z}_t) + \sum_{\tilde{k}=K_T+1}^K \text{Tr}(\mathbf{V}_{\tilde{k},T} \mathbf{Z}_t) + \sum_{q=1}^M \text{Tr}(\mathbf{V}_{q,T} \mathbf{Z}_t) + \sigma_{\tilde{n}_c}^2} \quad (37)$$

On the other hand, since the communication user  $\mathbf{U}_{k,R}$  has a direct link from the BS and the reflective passive elements of the hybrid STAR-RIS add a negligible contribution on the received signal determined in (20), the SINR of the user  $\mathbf{U}_{k,R}$  can be approximated as

$$R_{k,R} \approx \frac{\text{Tr}(\tilde{\mathbf{V}}_{k,R})}{\sum_{\tilde{k} \neq k}^{K_R} \text{Tr}(\tilde{\mathbf{V}}_{\tilde{k},R}) + \sum_{\tilde{k}=K_R+1}^K \text{Tr}(\tilde{\mathbf{V}}_{\tilde{k},R}) + \sum_{q=1}^M \text{Tr}(\tilde{\mathbf{V}}_{q,R}) + \sigma_c^2} \quad (38)$$

where  $\tilde{\mathbf{V}}_{k,R} = (\mathbf{g}_{k,R} \mathbf{w}_{k,R})^H (\mathbf{g}_{k,R} \mathbf{w}_{k,R})$ ,  $\tilde{\mathbf{V}}_{\tilde{k},R} = (\mathbf{g}_{k,R} \mathbf{w}_{\tilde{k},R})^H (\mathbf{g}_{k,R} \mathbf{w}_{\tilde{k},R})$  and  $\tilde{\mathbf{V}}_{q,R} = (\mathbf{g}_{k,R} \mathbf{w}_{q,R})^H (\mathbf{g}_{k,R} \mathbf{w}_{q,R})$ .

### C. Problem Formulation

To optimize the coefficients of the hybrid STAR-RIS the following problem that maximizes the minimum target SINR

under the communication SINR constraint is formulated.

$$(P1) \quad \max_{\Phi_t, \Phi_r} \min_{m,S} \gamma_{m,i} \quad (39a)$$

$$\text{s.t.} \quad |\mathbf{z}_r(n)| = 1, \quad \forall n \in \{1, \dots, N\} \quad (39b)$$

$$|\mathbf{z}_t(n)| \geq 1, \quad \forall n \in \{1, \dots, N\} \quad (39c)$$

$$R_{k,i} \geq R_{th} \quad (39d)$$

$$\text{Tr}(\mathbf{R}_x) \leq P_{\text{BS}} \quad (39e)$$

$$\text{Tr}(\mathbf{Z}_t) \leq P_A^2. \quad (39f)$$

Here  $R_{th}$  is the minimum SINR constraint for the communication users, while  $\mathbf{Z}_t = \mathbf{z}_t \mathbf{z}_t^H \in \mathbb{C}^{N \times 1}$ , subject to  $\text{rank}(\mathbf{Z}_t) = 1$  and  $\mathbf{Z}_t \succeq 0$ , and  $\mathbf{Z}_r = \mathbf{z}_r \mathbf{z}_r^H \in \mathbb{C}^{N \times 1}$ , subject to  $\text{rank}(\mathbf{Z}_r) = 1$  and  $\mathbf{Z}_r \succeq 0$ , where  $\mathbf{z}_t \in \mathbb{C}^{N \times 1}$  and  $\mathbf{z}_r \in \mathbb{C}^{N \times 1}$ , respectively. Here, it is obvious that problem (P1) is a non-convex QCQP problem, which can be transformed into a SDP problem using the semi-definite relaxation (SDR) approach via relaxing the constraints. Therefore, (P1) can be reformulated as

$$(P2) \quad \max_{\Phi_t, \Phi_r} \min_{m,S} \gamma_{m,i} \quad (40a)$$

$$\text{s.t.} \quad (39d), (39e), (39f) \quad (40b)$$

$$\mathbf{Z}_r \succeq 0 \quad (40c)$$

$$\mathbf{Z}_t \succeq 0. \quad (40d)$$

Next, (P2) can be reformulated as a linear matrix inequality (LMI) as follows

$$(P3) \quad \max_{\Phi_t, \Phi_r} \min_{m,S} \gamma_{m,i} \quad (41a)$$

$$\text{s.t.} \quad (39d), (39e), (39f), (40c), (40d) \quad (41b)$$

$$P_A (\beta_{\text{RIS}}^{m,T})^2 \text{Tr}(\mathbf{Q}_{m,T} \mathbf{Z}_t) \text{Tr}(\mathbf{R}_x) \geq \sum_{j \neq m}^{M_R} \text{Tr}((\mathbf{f}_{j,R}^H \mathbf{f}_{j,R})^2) \text{Tr}(\mathbf{R}_x) + \sum_{\tilde{m} \neq m}^{M_T} P_A^2 (\beta_{\text{RIS}}^{\tilde{m},T})^2 \text{Tr}(\mathbf{Q}_{\tilde{m},T} \mathbf{Z}_t) \text{Tr}(\mathbf{R}_x) + \sigma_{\tilde{n}_s}^2 \quad (41c)$$

$$(\beta_{\text{BS}}^{m,R})^2 \text{Tr}(\mathbf{R}_x) (\text{Tr}(\mathbf{A}_m \mathbf{A}_m^H)^2 + N \text{Tr}(\mathbf{Q}_{m,R} \mathbf{Z}_r)) \geq \sum_{\tilde{m} \neq m}^{M_R} (\beta_{\text{BS}}^{\tilde{m},R})^2 \text{Tr}(\mathbf{R}_x) (\text{Tr}(\mathbf{A}_{\tilde{m},R} \mathbf{A}_{\tilde{m},R}^H)^2 + N \text{Tr}(\mathbf{Q}_{\tilde{m},R} \mathbf{Z}_r)) + \sum_{j=1}^{M_T} P_A^2 (\beta_{\text{RIS}}^{j,T})^2 \text{Tr}(\mathbf{Q}_{j,T} \mathbf{Z}_t) \text{Tr}(\mathbf{R}_x) + \sigma_{\tilde{n}_s}^2. \quad (41d)$$

Here, the optimization problem (P3) can be efficiently solved with CVX solvers [37]. The complexity of solving the SDR problem (P3), which leverages the interior point method for a solution accuracy of  $\epsilon > 0$ , can be calculated as  $\mathcal{O}((K^{4.5} M^{4.5} + N^{4.5}) \log(1/\epsilon))$  [46]. However, the SDR solution does not always guarantee the rank-one solution

for the recovered  $\hat{\mathbf{Z}}_t$  and  $\hat{\mathbf{Z}}_r$  matrices. To address this, the eigenvalue decomposition [33] or Gaussian randomization [46] can be employed to obtain a feasible rank-one solution to the problem (41). At this point, the eigenvalue decomposition [33] is applied to recover the diagonal elements of  $\hat{\mathbf{Z}}_t$  and  $\hat{\mathbf{Z}}_r$  as  $\hat{\mathbf{z}}_t \in \mathbb{C}^{N \times 1}$  and  $\hat{\mathbf{z}}_r \in \mathbb{C}^{N \times 1}$ , respectively, where  $\hat{\mathbf{Z}}_t = \hat{\mathbf{z}}_t \hat{\mathbf{z}}_t^H$  and  $\hat{\mathbf{Z}}_r = \hat{\mathbf{z}}_r \hat{\mathbf{z}}_r^H$ .

Then the beamforming matrix is determined using optimal transmit beamforming via defining the overall beamforming matrix in (6) as  $\mathbf{W} \in \mathbb{C}^{T_x \times (K+M)} = [\mathbf{w}_{c,1}, \dots, \mathbf{w}_{c,K}, \mathbf{w}_{s,1}, \dots, \mathbf{w}_{s,M}]$ . Here,  $\mathbf{w}_{c,p}$  and  $\mathbf{w}_{s,q}$  are the beamforming vectors corresponding to  $p$ -th communication user and  $q$ -th sensing target, respectively. These beamforming vectors are defined as follows

$$\mathbf{w}_{c,p} = \sqrt{P_c} \frac{\tilde{\mathbf{h}}_{c,p}}{\|\tilde{\mathbf{h}}_{c,p}\|}, \quad \mathbf{w}_{s,q} = \sqrt{P_s} \frac{\tilde{\mathbf{h}}_{s,q}}{\|\tilde{\mathbf{h}}_{s,q}\|} \quad (42)$$

where  $\tilde{\mathbf{h}}_{c,p}$  is the overall channel for the  $p$ -th communication user and  $\tilde{\mathbf{h}}_{s,q}$  is the overall channel for  $q$ -th sensing target for  $p \in \{1, \dots, K\}$  and  $q \in \{1, \dots, M\}$ . Here, for a communication user on Side- $T$ ,  $\tilde{\mathbf{h}}_{c,p} = \mathbf{h}_{p,T} \Phi_t \mathbf{G}$  (19), while for those on Side- $R$ , it is  $\tilde{\mathbf{h}}_{c,p} = \mathbf{h}_{p,R} \Phi_r \mathbf{G} + \mathbf{g}_{p,R}$  (20). Similarly, for a sensing target on Side- $T$  (22),  $\tilde{\mathbf{h}}_{s,q} = \mathbf{b}(\varphi_{s,h}^{q,T}, \varphi_{s,v}^{q,T}) \Phi_t \mathbf{G}$ , while for ones on Side- $R$  (20), it is  $\tilde{\mathbf{h}}_{s,q} = \mathbf{a}(\theta_{s,h}^{q,R}, \theta_{s,v}^{q,R}) + \tilde{\mathbf{b}}(\varphi_{s,h}^{q,R}, \varphi_{s,v}^{q,R}) \Phi_r \mathbf{G}$ . Additionally, the transmit power for each communication user and sensing target is represented as  $P_c$  and  $P_s$ , respectively, where  $P_c = P_s = P_{BS}/(K+M)$ .

#### D. Cramer-Rao Bound (CRB) Analysis

In this section, to evaluate sensing performance of the targets, the CRB estimation for 2D AoDs of the targets has been investigated. To achieve this, first, the Fisher information matrix (FIM) is derived.

Let  $\boldsymbol{\zeta}_{m,i} \in \mathbb{C}^{4 \times 1} = [\varphi_{s,h}^{m,i}, \beta_{s,i}^{m,i}]^T$  be the vector of unknown parameters to be estimated that includes 2D AoDs of  $m$ th target on Side- $i$ ,  $\varphi_{s,i}^{m,i} \in \mathbb{C}^{1 \times 2}$  and its corresponding complex channel coefficient  $\beta_{s,i}^{m,i} \in \mathbb{C}^{1 \times 2}$ , where  $i \in \mathcal{S} = \{T, R\}$  and  $m \in \{1, \dots, M_i\}$ . For the target on the Side- $T$ ,  $\varphi_{s,h}^{m,T} = [\varphi_{s,h}^{m,T}, \varphi_{s,v}^{m,T}]$  and complex channel coefficient  $\beta_{s,i}^{m,T} = [\Re(\beta_{s,i}^{m,T}), \Im(\beta_{s,i}^{m,T})]$ . Then, in order to obtain the FIM, overall received echo signal in (23) is vectorized for  $\mathbf{u}_{m,T} = \beta_{s,i}^{m,T} \text{vec}(\mathbf{G}^H \Phi_t^H \mathbf{B}_m \Phi_t \mathbf{G} \mathbf{X})$ ,  $\tilde{\mathbf{n}}_{m,T} = \text{vec}(\tilde{\mathbf{N}}_s^{m,T})$  as follows

$$\mathbf{y}_s^{m,T} = \mathbf{u}_{m,T} + \tilde{\mathbf{n}}_{m,T}. \quad (43)$$

Therefore, the FIM for estimating  $\boldsymbol{\zeta}_{m,T}$  is constructed as [47]

$$\mathbf{J}_{m,T} = \begin{bmatrix} \mathbf{J}_{\varphi\varphi}^{m,T} & \mathbf{J}_{\varphi\beta}^{m,T} \\ \mathbf{J}_{\beta\varphi}^{m,T} & \mathbf{J}_{\beta\beta}^{m,T} \end{bmatrix}. \quad (44)$$

Then, utilizing (44), the CRB can be expressed as [47]

$$\text{CRB}(\varphi_{m,T}) = [\mathbf{J}_{\varphi\varphi}^{m,T} - \mathbf{J}_{\varphi\beta}^{m,T} (\mathbf{J}_{\beta\beta}^{m,T})^{-1} \mathbf{J}_{\beta\varphi}^{m,T}]^{-1} \quad (45)$$

where

$$\mathbf{J}_{m,T}(\delta, \omega) = \frac{2}{\sigma_{\tilde{\mathbf{n}}_s}^2} \Re \left\{ \frac{\partial \mathbf{u}_{m,T}^H}{\partial \boldsymbol{\zeta}_\delta} \frac{\partial \mathbf{u}_{m,T}}{\partial \boldsymbol{\zeta}_\omega} \right\} \quad \delta, \omega \in \{1, 2, 3, 4\} \quad (46)$$

Here,  $\mathbf{B}_m = \mathbf{b}^H(\varphi_{s,h}^{m,T}, \varphi_{s,v}^{m,T}) \mathbf{b}(\varphi_{s,h}^{m,T}, \varphi_{s,v}^{m,T})$

$$\begin{aligned} \frac{\partial \mathbf{u}_{m,T}}{\partial \varphi_{m,T}} &= \\ &[\beta_{\text{RIS}}^{m,T} \text{vec}(\mathbf{G}^H \Phi_t^H \dot{\mathbf{B}}_{\varphi_h}^m \Phi_t \mathbf{G} \mathbf{X}), \beta_{\text{RIS}}^{m,T} \text{vec}(\mathbf{G}^H \Phi_t^H \dot{\mathbf{B}}_{\varphi_v}^m \Phi_t \mathbf{G} \mathbf{X})] \end{aligned} \quad (47)$$

$$\frac{\partial \mathbf{u}_{m,T}}{\partial \beta_{m,T}} = \text{vec}(\mathbf{G}^H \Phi_t^H \mathbf{B}_m \Phi_t \mathbf{G} \mathbf{X}) [1 \ j] \quad (48)$$

where  $\dot{\mathbf{B}}_{\varphi_h}^m = \frac{\partial \mathbf{B}_m}{\partial \varphi_{s,h}^{m,T}}$  and  $\dot{\mathbf{B}}_{\varphi_v}^m = \frac{\partial \mathbf{B}_m}{\partial \varphi_{s,v}^{m,T}}$ . Therefore, since  $\mathbf{b}(\varphi_{s,h}^{m,T}, \varphi_{s,v}^{m,T})$  as expressed in (16), where  $\mathbf{k}_x$  and  $\mathbf{k}_y$  are vectors with scalar elements,  $\dot{\mathbf{B}}_{\varphi_h}^m$  and  $\dot{\mathbf{B}}_{\varphi_v}^m$  can be calculated as

$$\begin{aligned} \dot{\mathbf{B}}_{\varphi_h} &= j\eta_{\text{RIS}} (\mathbf{k}_x^H \cos(\varphi_{s,h}^{m,T}) \cos(\varphi_{s,v}^{m,T}) + \mathbf{k}_y^H \sin(\varphi_{s,h}^{m,T}) \sin(\varphi_{s,v}^{m,T})) \\ &\times (-\mathbf{b}(\varphi_{s,h}^{m,T}, \varphi_{s,v}^{m,T})^H \mathbf{b}(\varphi_{s,h}^{m,T}, \varphi_{s,v}^{m,T}) + \mathbf{b}(\varphi_{s,h}^{m,T}, \varphi_{s,v}^{m,T}) \mathbf{b}(\varphi_{s,h}^{m,T}, \varphi_{s,v}^{m,T})^H) \end{aligned} \quad (49)$$

$$\begin{aligned} \dot{\mathbf{B}}_{\varphi_v} &= j\eta_{\text{RIS}} (-\mathbf{k}_x^H \sin(\varphi_{s,h}^{m,T}) \sin(\varphi_{s,v}^{m,T}) + \mathbf{k}_y^H \sin(\varphi_{s,h}^{m,T}) \cos(\varphi_{s,v}^{m,T})) \\ &\times (-\mathbf{b}(\varphi_{s,h}^{m,T}, \varphi_{s,v}^{m,T})^H \mathbf{b}(\varphi_{s,h}^{m,T}, \varphi_{s,v}^{m,T}) + \mathbf{b}(\varphi_{s,h}^{m,T}, \varphi_{s,v}^{m,T}) \mathbf{b}(\varphi_{s,h}^{m,T}, \varphi_{s,v}^{m,T})^H) \end{aligned} \quad (50)$$

Let the overall signal be represented as  $\mathbf{F}_m = \mathbf{G}^H \Phi_t^H \mathbf{B}_m \Phi_t \mathbf{G} \mathbf{X}$ , while  $\dot{\mathbf{F}}_{\varphi_h} = \mathbf{G}^H \Phi_t^H \dot{\mathbf{B}}_{\varphi_h}^m \Phi_t \mathbf{G} \mathbf{X}$  and  $\dot{\mathbf{F}}_{\varphi_v} = \mathbf{G}^H \Phi_t^H \dot{\mathbf{B}}_{\varphi_v}^m \Phi_t \mathbf{G} \mathbf{X}$ . Therefore, the elements of the FIM can be defined as [28]

$$\begin{aligned} \mathbf{J}_{\varphi\varphi}^{m,T}(\mathbf{F}_m) &= \\ \frac{2L}{\sigma_{\tilde{\mathbf{n}}_s}^2} (\beta_{\text{RIS}}^{m,T})^2 \Re \left\{ \begin{bmatrix} \text{Tr}(\dot{\mathbf{F}}_{\varphi_h} \mathbf{R}_x \dot{\mathbf{F}}_{\varphi_h}^H) & \text{Tr}(\dot{\mathbf{F}}_{\varphi_h} \mathbf{R}_x \dot{\mathbf{F}}_{\varphi_v}^H) \\ \text{Tr}(\dot{\mathbf{F}}_{\varphi_v} \mathbf{R}_x \dot{\mathbf{F}}_{\varphi_h}^H) & \text{Tr}(\dot{\mathbf{F}}_{\varphi_v} \mathbf{R}_x \dot{\mathbf{F}}_{\varphi_v}^H) \end{bmatrix} \right\} \end{aligned} \quad (51)$$

$$\mathbf{J}_{\varphi\beta}^{m,T}(\mathbf{F}_m) = \frac{2L}{\sigma_{\tilde{\mathbf{n}}_s}^2} \Re \left\{ \begin{bmatrix} \beta_{\text{RIS}}^{m,T} \text{Tr}(\mathbf{F}_m \mathbf{R}_x \dot{\mathbf{F}}_{\varphi_h}^H) \\ \beta_{\text{RIS}}^{m,T} \text{Tr}(\mathbf{F}_m \mathbf{R}_x \dot{\mathbf{F}}_{\varphi_v}^H) \end{bmatrix} \begin{bmatrix} 1 & j \end{bmatrix} \right\} \quad (52)$$

$$\mathbf{J}_{\beta\beta}^{m,T}(\mathbf{F}_m) = \frac{2L}{\sigma_{\tilde{\mathbf{n}}_s}^2} \mathbf{I}_2 \text{Tr}(\mathbf{F}_m \mathbf{R}_x \mathbf{F}_m^H) \quad (53)$$

Then, the CRB of the  $m$ th distant target is obtained by substituting (51-53) into (45).

In similar way, the CRB of the sensing targets on Side- $R$  can be calculated for AoDs from BS to the target  $\mathbf{O}_{m,R}$   $\boldsymbol{\theta}^{m,R} = [\theta_{s,h}^{m,R}, \theta_{s,v}^{m,R}]$  and complex channel coefficient  $\beta^{m,R} = [\Re(\beta_{\text{BS}}^{m,R}), \Im(\beta_{\text{BS}}^{m,R})]$  via following (45-53) steps.

#### IV. SIMULATION RESULTS

In this section, Monte Carlo simulation results are provided to evaluate the sensing performance of the hybrid STAR-RIS-assisted ISAC scheme and the proposed optimization algorithm. Computer simulation results are conducted for a two-user and two-target scenario, where there is one user and one target located on each side ( $T, R$ ) of the hybrid STAR-RIS. Specifically, the user and target at Side- $R$  denoted as  $\mathbf{U}_R$  and  $\mathbf{O}_R$ , while those on Side- $T$  are referred to as  $\mathbf{U}_T$  and  $\mathbf{O}_T$ , respectively. Additionally, system parameters used in the simulations are listed in Table I.

TABLE I  
SYSTEM PARAMETERS

Notation	Parameter	Value
$f_c$	Operating frequency	3.315 GHz
$T_x$	Number of transmit/receive antennas at BS	8
$K$	Total number of communication users	2
$M$	Total number of sensing targets	2
$\kappa$	Rician factor	3 dB
$\sigma_{n_s}^2 = \sigma_{n_c}^2$	Noise power	-80 dBm
$L_c$	Coherence time length	100
$\alpha_0$	Reference path loss at 1 m	30 dB
$\rho$	Path loss exponent	2.2
$\Lambda$	RCS	100 m <sup>2</sup>
$\theta_h^R, \theta_v^R$	AoDs of target $O_R$	$\{35^\circ, 110^\circ\}$
$\varphi_h^T, \varphi_v^T$	AoDs of target $O_T$	$\{40^\circ, 108^\circ\}$
$d_{BS-RIS}$	Distance: BS-STAR-RIS	5 m
$d_{RIS-O_T}, d_{RIS-U_T}$	Distances: STAR-RIS- $O_T$ and STAR-RIS- $U_T$	$\{17, 18\}$ m
$d_{BS-O_R}, d_{RIS-O_R}$	Distances: BS- $O_R$ and STAR-RIS- $O_R$	$\{38, 41\}$ m
$d_{BS-U_R}, d_{RIS-U_R}$	Distances: BS- $U_R$ and STAR-RIS- $U_R$	$\{25, 27\}$ m

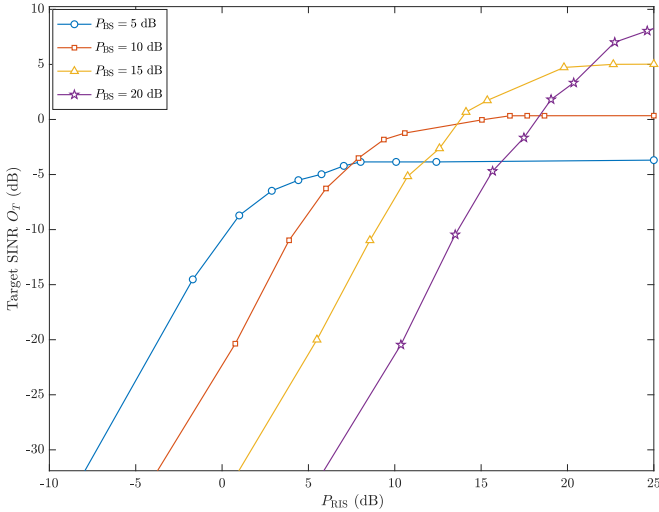


Fig. 3. SINR of target  $O_T$  versus power consumption at active STAR-RIS elements for  $N = 36$  and different  $P_{BS}$  values.

Fig. 3 presents the SINR of the target on Side- $T$ , denoted as  $O_T$ , for  $N = 36$  hybrid STAR-RIS elements with varying  $P_{RIS}$  due to increasing  $P_A$  and transmit power levels at the BS,  $P_{BS} = \{5, 10, 15, 20\}$  dB. The results clearly show that increasing  $P_{BS}$  enhances the SINR performance of the target  $O_T$ . On the other hand, higher  $P_{BS}$  values also lead to greater  $P_{RIS}$ , as discussed in (25). This highlights a fundamental trade-off between enhancing SINR and increasing the power consumption of the active STAR-RIS elements, where  $P_{BS}$  plays a crucial role in balancing the performance improvements with

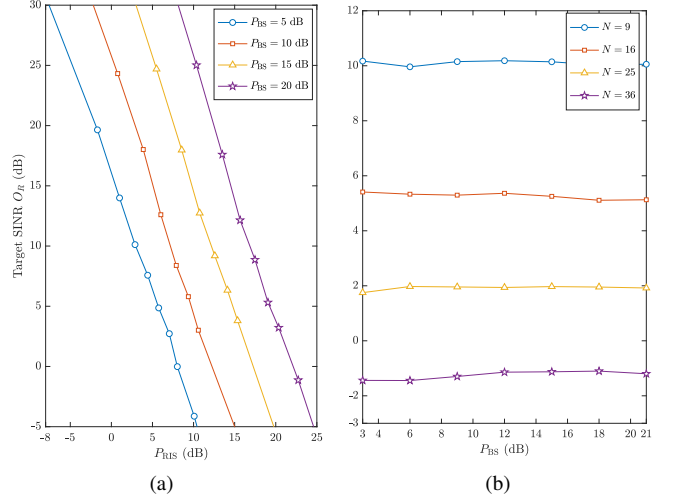


Fig. 4. SINR of target  $O_T$  for varying  $P_{RIS}$  (a) and  $P_{BS}$  (b).

power consumption. Moreover, it can be deduced from Fig. 3 that after a certain  $P_{RIS}$  value, the increased thermal noise from the active transmissive elements causes the target SINR values to saturate. This further supports that remaining at lower  $P_{RIS}$  range is significant for maintaining efficient target SINR performance.

In Fig. 4, the SINR of the target on Side- $R$ , denoted as  $O_R$ , is given for varying  $P_{RIS}$  (a) and  $P_{BS}$  (b) values. Fig. 4a), indicates a degradation in SINR of the target with increasing  $P_{RIS}$ . This effect can be attributed to the increase in power of the active elements that enhance the signal for the distant target  $O_T$ , which then serves as interference for  $O_R$ , as described in (35). Consequently, this interference leads to a reduction in the SINR of the target  $O_R$ .

On the other hand, in Fig. 4b), the SINR of the target  $O_R$  given for increasing  $P_{BS}$  values. The results indicate that the increased  $P_{BS}$  is equally distributed among all users and targets in the system, there is a negligible change in target SINR of  $O_R$ . This can be attributed to the fact that the increased  $P_{BS}$  is equally shared among all the users and targets in the system, it does not lead to significant improvements in the SINR of the target  $O_R$ . Additionally, from Fig. 4b), when  $P_{BS}$  is kept constant, an increase in  $N$  degrades the SINR of the target  $O_R$ . This can be explained by the fact that due to the direct link between the BS and  $O_R$ , and an increase in the number of passive elements  $N$  has a negligible effect on the SINR of  $O_R$ , unless the number of elements becomes significantly large. On the other hand, the SINR of the target  $O_T$  further improves with increasing number of active transmissive elements, which results in additional interference for  $O_R$ .

Fig. 5 presents the target SINR performance for the proposed hybrid STAR-RIS-aided ISAC system and fully-passive STAR-RIS-aided ISAC systems for varying number of STAR-RIS elements  $N$  at  $P_{BS} = 10$  dB. First, for a fair comparison, the transmit power of the reference passive RIS system is equated to the total power consumption of the proposed hybrid STAR-RIS assisted system, which includes the addi-

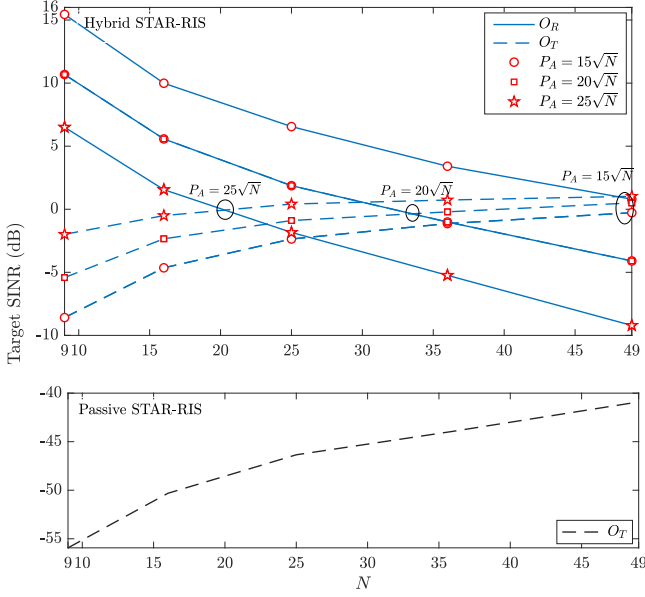


Fig. 5. SINR of the targets  $O_R$  and  $O_T$  for varying numbers of STAR-RIS elements  $N$ .

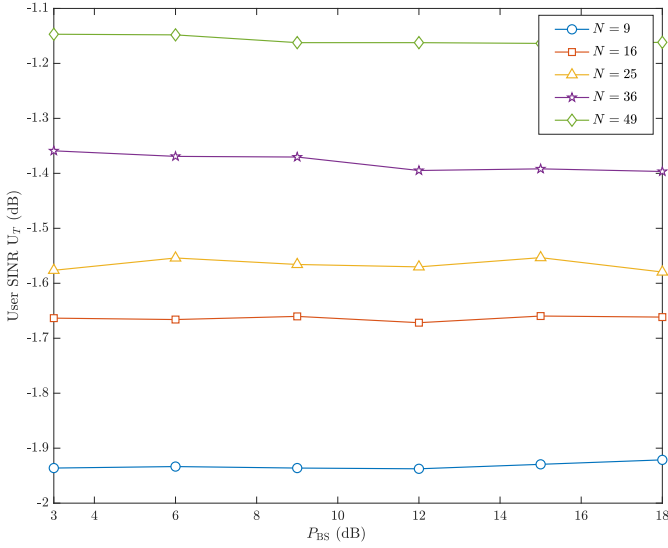


Fig. 6. SINR of the communication user  $U_T$  for varying  $N$ .

tional power consumption introduced by the use of active transmissive elements. The transmit power of the benchmark scheme is assumed to be  $P_{\text{Total}} = P_{BS} + P_{RIS}$ , where the amplification factor is set to  $P_A = 25\sqrt{N}$ . However, the results indicate that although  $P_{\text{Total}}$  reaches 16 dB for  $N = 49$  the reference passive STAR-RIS-assisted ISAC scheme is unable to mitigate the attenuation of the sensing signal caused by multi-hop transmission. In contrast, the hybrid STAR-RIS-aided ISAC system outperforms the benchmark, demonstrating a significant improvement in target SINR performance. This improvement can be attributed to the amplifying capability of the transmissive elements in the proposed hybrid STAR-RIS structure, which contrasts with the passive-only reflection/transmission characteristics of the benchmark scheme.

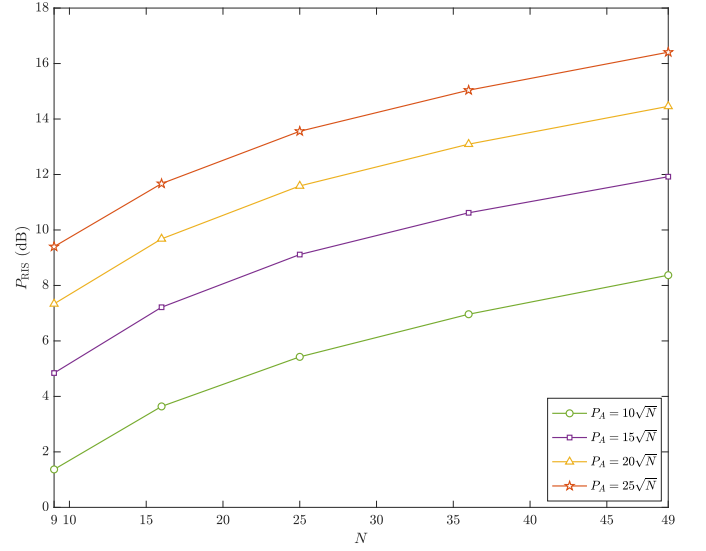


Fig. 7. Power consumption of active transmissive elements  $P_{RIS}$  at  $P_{BS} = 10$  dB for varying  $N$ .

Additionally, as illustrated in the Fig. 5, for the proposed hybrid STAR-RIS-aided ISAC scheme, increasing  $N$  improves the SINR performance of the target  $O_T$ . However, since the enhanced signal of the target  $O_T$  acts as interference for target  $O_R$ , it simultaneously degrades the SINR of  $O_R$ , which aligns with the results shown in Figs. 3-4. Moreover, the results indicate that increasing the overall amplification factor  $P_A$  further enhances the SINR of the target  $O_T$  while degrading the SINR performance of the target  $O_R$ . These results suggest a fair SINR distribution between the targets on both sides for different  $N$  values. Specifically, the SINR of targets  $O_R$  and  $O_T$  nearly reach equilibrium for varying  $P_A$  values. A balanced target SINR is achieved between both sides at approximately  $P_A = 15\sqrt{N}$  around  $N = 49$ , for  $P_A = 20\sqrt{N}$  when  $N = 34$ , and for  $P_A = 25\sqrt{N}$  when  $N = 20$ . This suggests that for smaller amplification factors  $P_A$  a hybrid STAR-RIS with a larger  $N$  is needed to maintain a balanced SINR distribution between both sides.

In Fig. 6, the SINR performance of the communication user on Side-T,  $U_T$  for varying  $N$  is shown. As anticipated, the results indicate significant improvement in SINR performance of the user  $U_T$  as  $N$  increases. On the other hand, an increase in the  $P_{BS}$  dB does not yield in a noticeable enhancement in the SINR performance of the user  $U_T$ . It can be deduced from Fig. 6 that since signal enhancement on Side-T is achieved via active transmissive elements, the transmit power at the BS, as a result,  $P_{BS}$ , has an almost negligible effect on the user SINR on Side-T.

In Fig. 7, the power consumption of active transmissive elements  $P_{RIS}$  is given for varying numbers of hybrid STAR-RIS elements  $N$  and  $P_A$ . As corroborated by (25) and the results presented in Figs. 5-6 is obvious that an increase in  $N$  leads to higher  $P_{RIS}$ . Particularly, for a certain  $N$  value, a  $5\sqrt{N}$  increase in  $P_A$  results in 2 dB increase in  $P_{RIS}$ . These results illustrate a trade-off between achieving high target SINR and user SINR while managing power consumption of the active

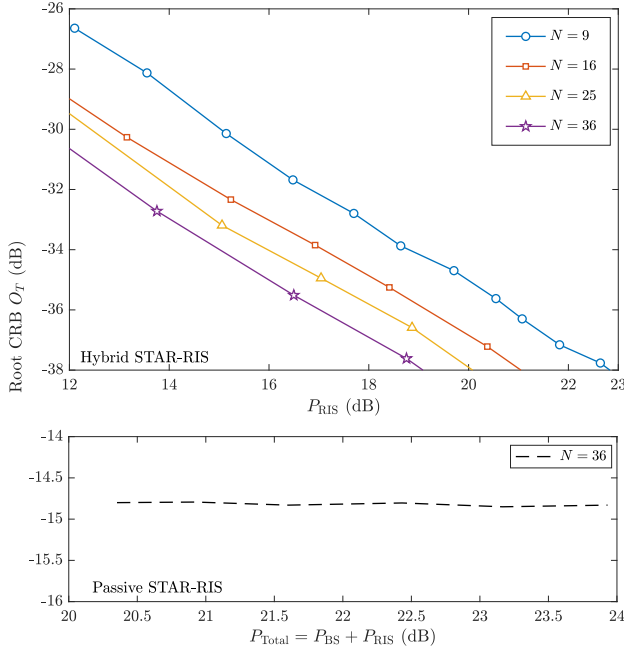


Fig. 8. Root CRB of target  $O_T$  versus power consumption of active transmissive elements  $P_{RIS}$  for varying numbers of hybrid STAR-RIS elements  $N$ .

transmissive elements.

Fig. 8 illustrates the root CRB estimation of 2D AoDs of the target  $O_T$  for the proposed hybrid STAR-RIS and reference passive STAR-RIS-assisted ISAC schemes for different  $N$  values at  $P_{BS} = 20$  dB. Here, although the benchmark passive STAR-RIS-aided ISAC scheme is evaluated for the overall power  $P_{Total} = P_{BS} + P_{RIS}$ , it achieves a negligible improvement in root CRB performance compared to hybrid STAR-RIS-assisted ISAC scheme. This limited performance improvement of the passive STAR-RIS-assisted scheme is due to the multi-user and multi-target structure, where an increase in  $P_{Total}$  equally impacts both sensing targets and communication users (42), leading to minimal changes in performance. On the other hand, for the proposed hybrid STAR-RIS-assisted ISAC scheme, as  $N$  increases, there is an noticeable improvement in the root CRB estimation. This can be attributed to enhanced sensing signal power and an accompanying rise in  $P_{RIS}$  as  $N$  increases. Consequently, while increasing overall transmit power impacts sensing targets and communication users equally, increasing the power of active transmissive elements in the hybrid STAR-RIS scheme specifically improves the performance of the sensing target and the communication user on Side-T.

In Fig. 9, the root CRB estimation for AoDs of the target  $O_R$  is given for varying  $P_{BS}$ . It is apparent from the results that an increase in  $P_{BS}$  and  $N$  improve the CRB estimation of AoDs of the target  $O_R$ . It is also observed that when root CRB is kept constant, a hybrid STAR-RIS comprising a higher number of  $N$  elements necessitate a lower  $P_{BS}$  at the BS.

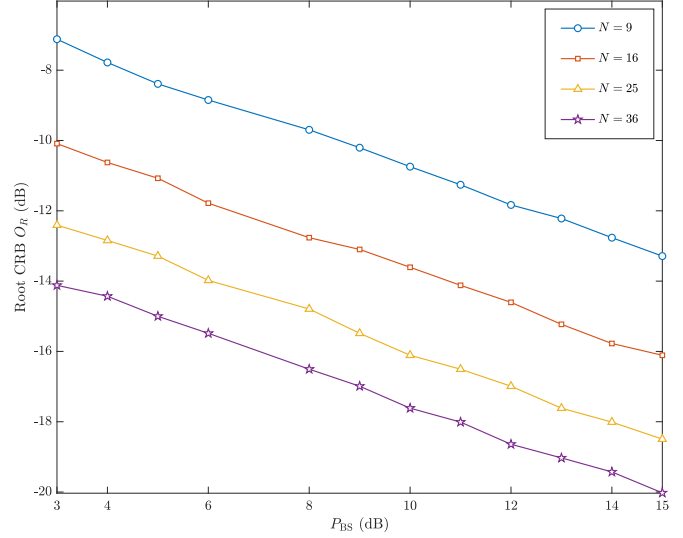


Fig. 9. Root CRB of target  $O_R$  versus  $P_{BS}$  for varying numbers of hybrid STAR-RIS elements  $N$ .

## V. CONCLUSION

This paper has proposed a novel hybrid STAR-RIS-aided ISAC transmission scheme with full-space communication and sensing capabilities for multi-user and multi-target scenarios. In the proposed scheme, to address significant path attenuation resulting from multi-hop transmission, low-power active transmissive elements have been considered at the hybrid STAR-RIS that introduce considerable power consumption. Moreover, sensing performance metrics including target SINR and CRB for 2D AoDs estimation have been derived. An SDR-based optimization algorithm has been developed to maximize the minimum SINR of the targets by optimizing transmissive and reflective coefficients of the hybrid STAR-RIS elements. Furthermore, to evaluate communication and sensing performance of the system and illustrate the effectiveness of the proposed algorithm, a comprehensive simulations have been conducted.

## REFERENCES

- [1] Recommendation ITU-R M.2160-0, "Framework and overall objectives of the future development of IMT for 2030 and beyond," Tech. Rep., Nov. 2023.
- [2] F. Liu, Y. Cui, C. Masouros, J. Xu, T. X. Han, Y. C. Eldar, and S. Buzzi, "Integrated sensing and communications: Toward dual-functional wireless networks for 6G and beyond," *IEEE J. Sel. Areas Commun.*, vol. 40, no. 6, pp. 1728–1767, Mar. 2022.
- [3] Y. Cui, F. Liu, X. Jing, and J. Mu, "Integrating sensing and communications for ubiquitous IoT: Applications, trends, and challenges," *IEEE Netw.*, vol. 35, no. 5, pp. 158–167, Nov. 2021.
- [4] F. Liu, C. Masouros, A. P. Petropulu, H. Griffiths, and L. Hanzo, "Joint radar and communication design: Applications, state-of-the-art, and the road ahead," *IEEE Trans. Commun.*, vol. 68, no. 6, pp. 3834–3862, Feb. 2020.
- [5] J. A. Zhang, F. Liu, C. Masouros, R. W. Heath, Z. Feng, L. Zheng, and A. Petropulu, "An overview of signal processing techniques for joint communication and radar sensing," *IEEE J. Sel. Topics Signal Process.*, vol. 15, no. 6, pp. 1295–1315, Sep. 2021.
- [6] A. Hassanien, M. G. Amin, Y. D. Zhang, and F. Ahmad, "Signaling strategies for dual-function radar communications: An overview," *IEEE Aerosp. Electron. Syst. Mag.*, vol. 31, no. 10, pp. 36–45, Oct. 2016.

- [7] E. Basar, M. Di Renzo, J. De Rosny, M. Debbah, M.-S. Alouini, and R. Zhang, "Wireless communications through reconfigurable intelligent surfaces," *IEEE Access*, vol. 7, pp. 116 753–116 773, Aug. 2019.
- [8] E. Basar, G. C. Alexandropoulos, Y. Liu, Q. Wu, S. Jin, C. Yuen, O. A. Dobre, and R. Schober, "Reconfigurable intelligent surfaces for 6G: Emerging hardware architectures, applications, and open challenges," *IEEE Veh. Technol. Mag. (to appear)*, June 2024.
- [9] M. Di Renzo, A. Zappone, M. Debbah, M.-S. Alouini, C. Yuen, J. De Rosny, and S. Tretjakov, "Smart radio environments empowered by reconfigurable intelligent surfaces: How it works, state of research, and the road ahead," *IEEE J. Sel. Areas Commun.*, vol. 38, no. 11, pp. 2450–2525, July 2020.
- [10] Q. Wu, B. Zheng, C. You, L. Zhu, K. Shen, X. Shao, W. Mei, B. Di, H. Zhang, E. Basar et al., "Intelligent surfaces empowered wireless network: Recent advances and the road to 6G," *Proc. IEEE (Early Access)*, Apr. 2024.
- [11] C. Huang, A. Zappone, G. C. Alexandropoulos, M. Debbah, and C. Yuen, "Reconfigurable intelligent surfaces for energy efficiency in wireless communication," *IEEE Trans. Wireless Commun.*, vol. 18, no. 8, pp. 4157–4170, June 2019.
- [12] E. Basar, "Transmission through large intelligent surfaces: A new frontier in wireless communications," in *2019 European Conference on Networks and Communications (EuCNC)*. IEEE, June 2019, pp. 112–117.
- [13] S. Zhang and R. Zhang, "Capacity characterization for intelligent reflecting surface aided MIMO communication," *IEEE J. Sel. Areas Commun.*, vol. 38, no. 8, pp. 1823–1838, June 2020.
- [14] Q. Wu and R. Zhang, "Intelligent reflecting surface enhanced wireless network via joint active and passive beamforming," *IEEE Trans. Wireless Commun.*, vol. 18, no. 11, pp. 5394–5409, Aug. 2019.
- [15] J. Chen, Y.-C. Liang, Y. Pei, and H. Guo, "Intelligent reflecting surface: A programmable wireless environment for physical layer security," *IEEE Access*, vol. 7, pp. 82 599–82 612, June 2019.
- [16] E. Basar and H. V. Poor, "Present and future of reconfigurable intelligent surface-empowered communications [perspectives]," *IEEE Signal Process. Mag.*, vol. 38, no. 6, pp. 146–152, Oct. 2021.
- [17] S. W. Ellingson, "Path loss in reconfigurable intelligent surface-enabled channels," in *IEEE 32nd Annual International Symposium on Personal, Indoor and Mobile Radio Communications (PIMRC)*. IEEE, Oct. 2021, pp. 829–835.
- [18] Z. Zhang, L. Dai, X. Chen, C. Liu, F. Yang, R. Schober, and H. V. Poor, "Active RIS vs. passive RIS: Which will prevail in 6G?" *IEEE Trans. Commun.*, vol. 71, no. 3, pp. 1707–1725, Dec. 2022.
- [19] K. Zhi, C. Pan, H. Ren, K. K. Chai, and M. El-kashlan, "Active RIS versus passive RIS: Which is superior with the same power budget?" *IEEE Commun. Lett.*, vol. 26, no. 5, pp. 1150–1154, Mar. 2022.
- [20] Z. Yigit, E. Basar, M. Wen, and I. Altunbas, "Hybrid reflection modulation," *IEEE Trans. Wireless Commun.*, vol. 22, no. 6, pp. 4106–4116, Nov. 2022.
- [21] R. Long, Y.-C. Liang, Y. Pei, and E. G. Larsson, "Active reconfigurable intelligent surface-aided wireless communications," *IEEE Trans. Wireless Commun.*, vol. 20, no. 8, pp. 4962–4975, Mar. 2021.
- [22] K. K. Kishor and S. V. Hum, "An amplifying reconfigurable reflectarray antenna," *IEEE Trans. Antennas Propag.*, vol. 60, no. 1, pp. 197–205, Sep. 2011.
- [23] X. Mu, Y. Liu, L. Guo, J. Lin, and R. Schober, "Simultaneously transmitting and reflecting (STAR) RIS aided wireless communications," *IEEE Trans. Wireless Commun.*, vol. 21, no. 5, pp. 3083–3098, Oct. 2021.
- [24] J. Xu, J. Zuo, J. T. Zhou, and Y. Liu, "Active simultaneously transmitting and reflecting (STAR)-RISs: Modelling and analysis," *IEEE Commun. Lett.*, vol. 27, no. 9, pp. 2466 – 2470, June 2023.
- [25] A. M. Elbir, K. V. Mishra, M. B. Shankar, and S. Chatzinotas, "The rise of intelligent reflecting surfaces in integrated sensing and communications paradigms," *IEEE Netw.*, vol. 37, no. 6, pp. 224–231, Dec. 2022.
- [26] R. Liu, M. Li, H. Luo, Q. Liu, and A. L. Swindlehurst, "Integrated sensing and communication with reconfigurable intelligent surfaces: Opportunities, applications, and future directions," *IEEE Wireless Commun.*, vol. 30, no. 1, pp. 50–57, Feb. 2023.
- [27] S. P. Chepuri, N. Shlezinger, F. Liu, G. C. Alexandropoulos, S. Buzzi, and Y. C. Eldar, "Integrated sensing and communications with reconfigurable intelligent surfaces: From signal modeling to processing," *IEEE Signal Process. Mag.*, vol. 40, no. 6, pp. 41–62, Sep. 2023.
- [28] X. Song, J. Xu, F. Liu, T. X. Han, and Y. C. Eldar, "Intelligent reflecting surface enabled sensing: Cramér-rao bound optimization," *IEEE Trans. Signal Process.*, vol. 71, pp. 2011–2026, May 2023.
- [29] Z. Xing, R. Wang, and X. Yuan, "Joint active and passive beamforming design for reconfigurable intelligent surface enabled integrated sensing and communication," *IEEE Trans. Commun.*, vol. 71, no. 4, pp. 2457 – 2474, Feb. 2023.
- [30] R. P. Sankar, S. P. Chepuri, and Y. C. Eldar, "Beamforming in integrated sensing and communication systems with reconfigurable intelligent surfaces," *IEEE Trans. Wireless Commun.*, vol. 23, no. 5, pp. 4017–4031, Sep. 2023.
- [31] Z. Yu, H. Ren, C. Pan, G. Zhou, B. Wang, M. Dong, and J. Wang, "Active RIS aided ISAC systems: Beamforming design and performance analysis," *IEEE Trans. Commun.*, vol. 72, no. 3, pp. 1578 – 1595, Nov. 2023.
- [32] Q. Zhu, M. Li, R. Liu, and Q. Liu, "Joint transceiver beamforming and reflecting design for active RIS-aided ISAC systems," *IEEE Trans. Veh. Technol.*, vol. 72, no. 7, pp. 9636–9640, Feb. 2023.
- [33] Z. Wang, X. Mu, and Y. Liu, "STARS enabled integrated sensing and communications," *IEEE Trans. Wireless Commun.*, vol. 22, no. 10, pp. 6750 – 6765, Feb. 2023.
- [34] Z. Zhang, Y. Liu, Z. Wang, and J. Chen, "STARS-ISAC: How many sensors do we need?" *IEEE Trans. Wireless Commun.*, vol. 23, no. 2, pp. 1085 – 1099, June 2023.
- [35] M. Li, S. Zhang, Y. Ge, Z. integrated sensing and communication over high mobility scenario," *EEE Trans. Commun.*, volume=72, number=8, pages=4788 - 4802, year=Aug. 2024, publisher=IEEE.
- [36] Z. Zhang, W. Chen, Q. Wu, Z. Li, X. Zhu, and J. Yuan, "Intelligent omni surfaces assisted integrated multi-target sensing and multi-user MIMO communications," *IEEE Trans. Commun.*, Mar. 2024 (Early Access).
- [37] M. Grant and S. Boyd, "CVX: Matlab software for disciplined convex programming, version 2.1," <https://cvxr.com/cvx>, Mar. 2014.
- [38] M. Rihan, A. Zappone, S. Buzzi, G. Fodor, and M. Debbah, "Passive vs. active reconfigurable intelligent surfaces for integrated sensing and communication: challenges and opportunities," *IEEE Network*, vol. 38, no. 3, pp. 218 – 226, Apr. 2024.
- [39] Z. Liu, S. Aditya, H. Li, and B. Clerckx, "Joint transmit and receive beamforming design in full-duplex integrated sensing and communications," *IEEE J. Sel. Areas Commun.*, vol. 41, no. 9, pp. 2907–2919, June 2023.
- [40] J. Xu, X. Mu, J. T. Zhou, and Y. Liu, "Simultaneously transmitting and reflecting (STAR)-RISs: Are they applicable to dual-sided incidence?" *IEEE Wireless Commun. Lett.*, vol. 12, no. 1, pp. 129–133, Nov. 2022.
- [41] L. G. De Oliveira, B. Nuss, M. B. Alabd, A. Diewald, M. Pauli, and T. Zwick, "Joint radar-communication systems: Modulation schemes and system design," *IEEE Trans. Microw. Theory Techn.*, vol. 70, no. 3, pp. 1521–1551, Nov. 2021.
- [42] J. G. Proakis and M. Salehi, *Fundamentals of Communication Systems*. Pearson Education, 2007.
- [43] X. Shao, C. You, W. Ma, X. Chen, and R. Zhang, "Target sensing with intelligent reflecting surface: Architecture and performance," *IEEE J. Sel. Areas Commun.*, vol. 40, no. 7, pp. 2070–2084, Mar. 2022.
- [44] X. Meng, F. Liu, S. Lu, S. P. Chepuri, and C. Masouros, "RIS-assisted integrated sensing and communications: A subspace rotation approach," in *2023 IEEE Radar Conference (RadarConf23)*. IEEE, May 2023, pp. 1–6.
- [45] X.-D. Zhang, *Matrix analysis and applications*. Cambridge University Press, 2017.
- [46] Z.-Q. Luo, W.-K. Ma, A. M.-C. So, Y. Ye, and S. Zhang, "Semidefinite relaxation of quadratic optimization problems," *IEEE Signal Process. Mag.*, vol. 27, no. 3, pp. 20–34, May 2010.
- [47] I. Bekkerman and J. Tabrikian, "Target detection and localization using MIMO radars and sonars," *IEEE Trans. Signal Process.*, vol. 54, no. 10, pp. 3873–3883, Sep. 2006.